ACTA MEDICA (HRADEC KRÁLOVÉ)

2016, Vol. 59, No. 2

CONTENTS

ORIGINAL ARTICLES

CASE REPORTS

ORIGINAL ARTICLE

Does Simple Steatosis Affect Liver Regeneration after Partial Hepatectomy in Rats?

Tomáš Garnol, Otto Kučera[*], Pavla Staňková, Halka Lotková, Zuzana Červinková

Department of Physiology, Charles University in Prague, Faculty of Medicine in Hradec Králové, Hradec Králové, Czech Republic
* Corresponding author: Charles University in Prague, Faculty of Medicine in Hradec Králové, Šimkova 870, 500 38 Hradec Králové 1, Czech Republic; e-mail: kucerao@lfhk.cuni.cz

Summary: Aim: The aim of our study was to assess whether simple steatosis impairs liver regeneration after partial hepatectomy (PHx) in rats. Methods: Male Sprague–Dawley rats were fed a standard diet (ST-1, 10% kcal fat) and high-fat diet (HFD, 71% kcal fat) for 6 weeks. Then the rats were submitted to 2/3 PHx and animals were sacrificed 24, 48 or 72 h after PHx. Serum biochemistry, respiration of mitochondria in liver homogenate, hepatic oxidative stress markers, selected cytokines and DNA content were measured, and histopathological samples were prepared. Liver regeneration was evaluated by incorporation of bromodeoxyuridine (BrdU) to hepatocyte DNA. Results: HFD induced simple microvesicular liver steatosis. PHx caused elevation of serum markers of liver injury in both groups; however, an increase in these parameters was delayed in HFD group. Hepatic content of reduced glutathione was significantly increased in both groups after PHx. There were no significant changes in activities of respiratory complexes I and II (state 3). Relative and absolute liver weights, total DNA content, and DNA synthesis exerted very similar changes in both ST-1 and HFD groups after PHx. Conclusion: PHx-induced regeneration of the rat liver with simple steatosis was not significantly affected when compared to the lean liver.

Keywords: *Fatty liver; Liver regeneration; Partial hepatectomy*

Introduction

The liver has a unique and remarkable capacity for self-renewal after its damage. This regenerative potential is essential for survival after liver injury induced by toxic substances, viral infections, metabolic and immune dysfunctions and in response to surgical removal of a part of liver tissue (1, 2). Liver regeneration is most commonly studied by performing partial hepatectomy (PHx); the classical model represents removal of 2/3 of the liver mass in rodents as described by Higgins and Anderson (3). Advantage of PHx model of liver regeneration in comparison with other regenerative stimuli is the absence of injury to the remnant of liver tissue after surgery. Liver regeneration after partial hepatectomy is a very complex and well-orchestrated process associated with signaling cascades involving growth factors, cytokines, matrix remodeling, several feedbacks of stimulation and inhibition of growth related signals, and metabolic changes (4–6). Nevertheless, the fully integrated understanding of the mechanisms involved in the regulation of liver regeneration remains to be elucidated. The signals responsible for initiation and especially termination of liver regeneration are not completely defined yet (7). The interest to understand liver regeneration pushes not only ambition to understand this unique process of well controlled tissue proliferation but also clinical practice. Resection of liver for different reasons (primary and metastatic tumors, living donor of liver grafts for transplantation, etc.) has become a common clinical practice. The success of recovery and renewal of liver functions depends on the regeneration of the liver remnant. Pre-existing pathological abnormalities among which hepatic steatosis is one of the most frequent disorders may significantly deteriorate the course of liver regeneration after surgical resection and regeneration of steatotic graft after liver transplantation (8, 9).

Non-alcoholic fatty liver disease (NAFLD) is the most frequent hepatic disorder in the Western countries and its prevalence is still increasing (10). NAFLD refers to a wide spectrum of liver damages, ranging from simple steatosis to non-alcoholic steatohepatitis (NASH), advanced fibrosis, and cirrhosis. As described by Chalasani and coworkers the definition of NAFLD requires that firstly there is evidence of hepatic steatosis, either by imaging or by histology and secondly there are no causes for secondary hepatic fat accumulation such as significant alcohol consumption, use of steatogenic medication, or hereditary disorders (11).

NAFLD is associated with mitochondrial oxidative alterations (12), increased production of reactive oxygen and nitrogen species and decreased liver content of reduced glutathione (GSH) (13, 14). Accumulating evidence indi-

http://dx.doi.org/10.14712/18059694.2016.87

cates that mitochondrial dysfunction participates as a key player in the pathophysiology of NAFLD (15). Besides ultrastructural changes (16) and depletion of mitochondrial DNA (17, 18), mitochondrial dysfunction includes altered activities of respiratory complexes and decreased capacity for ATP synthesis (19, 20). Complex I (NADH:ubiquinone oxidoreductase) and complex II (succinate-ubiquinone oxidoreductase) are two respiratory complexes through which electrons enter respiratory chain. Their damage affects mitochondrial energy production and moreover dysfunction of complex I leads to considerable generation of reactive oxygen species (ROS).

There are several studies focused on regeneration of the liver affected by NAFLD with inconsistent results. There is evidence about impaired functional recovery and hepatocellular regeneration of the liver affected by steatosis after PHx in rats (21, 22). Similar results were found also in humans. Hepatic steatosis impairs liver regeneration as is reflected by the declining regeneration markers in patients with an increasing degree of steatosis (23). Patients with steatosis had an up to two-fold increased risk of postoperative complications, and those with excessive steatosis had an almost threefold increased risk of death after major hepatic resection (24). On the contrary other authors did not see impaired regenerative response of steatotic liver in rats after partial hepatectomy (25, 26). Cho and coworkers document that mild hepatic steatosis is not a major risk factor for hepatectomy, and that regenerative power is not impaired in living liver donors (27). To clarify the ability of steatotic liver to regenerate is important for clinical practice, e.g. for decision if the liver affected by NAFLD could be used for transplantation. The aim of our study was to evaluate whether simple steatosis affects the early course of liver regeneration after PHx. Important limiting step of liver regeneration is sufficient energy availability. Therefore we decided to assess in addition to the markers of liver injury and regeneration also oxygen uptake by mitochondria in liver homogenates.

Materials and Methods

Experimental design

Male Sprague–Dawley rats (AnLab, Prague, Czech Republic) with initial body weight of 240 ± 20 g were used throughout the study. The rats were housed at 22 ± 2 °C, 55 ± 10% humidity, air exchange 10 times/h and 12 h light–dark cycle. The animals had free access to tap water and different diets as described below. In accordance with Czech legislation, all animals received care according to the guidelines set out by the Animal-Welfare Body of the Charles University, Prague, Czech Republic, and the International Guiding Principles for Biomedical Research Involving Animals and our study was approved by this committee and by the Ministry of Education, Youth and Sports (MSMT 18324/2008-30).

Rats were fed *ad libitum* a standard pelleted diet (DOS 2B, Velaz, Prague, Czech Republic; 10% energy fat, 30% energy proteins, 60% energy saccharides, ST-1) or high-fat diet (HFD; 71% energy fat, 18% energy proteins, 11% energy saccharides) according to Lieber (28) modified by Kučera (14) for 6 weeks. Then the animals were submitted to 2/3 partial hepatectomy (n = 6 in each group) (65–70% of the liver tissue was removed comprising left lateral and median lobules of the liver) described by Higgins and Anderson (3) or laparotomy (sham operation, LAP, n = 4). Animals were sacrificed 24, 48 or 72 hours after PHx or LAP by exsanguination from aortic bifurcation and liver samples were collected for analyses. High-fat diet was prepared from ingredients purchased from MP Biomedicals (Solon, OH, USA). All chemicals, unless otherwise mentioned, were of analytical grade and were obtained from Sigma-Aldrich. After starvation for 14 h, the animals were sacrificed and liver and serum samples were taken. Samples for consequent evaluation were immediately frozen in liquid nitrogen and stored at −80 °C until analysis.

Serum biochemical measurements

Serum concentrations of total bilirubin, and activities of alanine aminotransferase (ALT), aspartate aminotransferase (AST) and alkaline phosphatase (ALP) were determined by routine laboratory methods (commercial sets, Roche Diagnostics) on Cobas Integra 800 (Roche Diagnostics) in the Institute for Clinical Biochemistry and Diagnostics, University Hospital in Hradec Králové.

Measurement of oxygen uptake by mitochondria in liver homogenate

Rat liver tissue was homogenized as previously described and oxygen consumption in liver homogenate (n = 3–4) was measured by a high-resolution respirometry using Oxygraph 2k (Oroboros Instruments, Innsbruck, Austria) (29, 30). The rate of oxygen consumption was evaluated using Oroboros DatLab 4 software and expressed as nmol oxygen/s/mg protein. Respiratory control index (RCI) for complex II substrates was calculated.

Determination of glutathione

Liver homogenate was added into cold 10% metaphosphoric acid, shaken and centrifuged (20,000 ×g, 10 min, 4 °C). Glutathione in the supernatant was analyzed by a modified fluorimetric method (31, 32). Briefly, reduced (GSH) an oxidized (GSSG) glutathione was allowed to react with o-phthalaldehyde in phosphate buffer, and the fluorimetric detection was carried out (λ_{Ex} = 340 nm, λ_{Em} = 420 nm).

Determination of tissue triacylglycerols, cholesterol and DNA

Lipids from rat livers were prepared using chloroform-methanol extraction (33). Total cholesterol and triacylglycerols (TAG) were measured using commercial kits (Roche Diagnostics GmbH, Mannheim, Germany). DNA was determined by means of the diphenylamine reagent according to Burton (34).

Determination of serum and liver tissue cytokines and hepatic malondialdehyde

Liver samples were homogenized in RIPA buffer, centrifuged (10,000 ×g) and the supernatant was collected. Protein content in the sample was determined by the method of Bradford (35) using bovine serum albumin as a standard. Concentrations of liver interleukin-6 (IL-6) and transforming growth factor-β1 (TGF-β1) in the supernatant were measured by enzyme linked immunosorbent assay (ELISA) (BMS625, BMS623, Bender MedSystems, Vienna, Austria). Total tissue malondialdehyde (MDA) was analyzed using a slightly modified method of Pilz (36). Briefly, derivatization with 2,4-dinitrophenylhydrazine was performed after an alkaline hydrolysis, and subsequent reversed-phase high-performance liquid chromatography (Agilent, Palo Alto, CA, USA).

Liver histology, bromodeoxyuridine staining and its quantification

Liver samples were taken immediately after the rats were sacrificed and fixed by immersion in 4% neutral formaldehyde. Paraffin sections were stained with hematoxylin & eosin. Fat accumulation in hepatocytes was confirmed by staining of formaldehyde-fixed frozen liver sections with oil red.

The immunohistochemical analysis of bromodeoxyuridine(BrdU)-stained samples was performed on paraffin sections of liver tissue (6 µm thick) as described previously (37). Quantification of BrdU-positive nuclei was performed in at least 10 microscope fields (10× objective magnification) in each section using NIS-Elements AR 2.30 (Nikon, Lewisville, TX).

Statistical analysis

The results are expressed as the mean ± SD. Analyses were performed using Graph-Pad Prism 4.03 software (Graph Pad Software, San Diego, CA, USA). First, normality was tested by Kolmogorov-Smirnov test. In normal data, comparisons were made among the groups using ANOVA followed by Tukey-Kramer's post hoc test. In the case of non-Gaussian distribution, non-parametric Kruskal-Wallis test and Dunn's post hoc test were used. $P < 0.05$ was considered statistically significant. Because there were not significant differences between control non-operated groups and laparotomized groups in either ST-1 or HFD feedings, respectively, we do not present results of sham-operated groups.

Results

Serum characteristics

As shown in table 1, PHx induced mild injury to the liver as documented by increased activities of ALT (24 h, $p < 0.001$), AST (24 and 48 h, $p < 0.001$ and 0.05, respectively) and ALP (24 and 48 h, $p < 0.05$) in ST-1 rats. In HFD animals, elevation of markers of liver injury was significantly delayed when compared to ST-1 (ALT 72 h, $p < 0.05$; ALP 48 and 72 h, $p < 0.05$ and 0.001, respectively; total bilirubin concentration 72 h, $p < 0.05$).

Histological parameters

Livers of rats fed by HFD showed simple microvesicular steatosis without inflammatory infiltrate, hepatocyte necrosis or fibrosis (data not shown). PHx induced regenerative response of hepatocytes which was visualized by staining of the incorporation of BrdU in hepatocyte DNA (Fig 1A-D). Semiquantitative analysis of BrdU-positive nuclei (Fig. 2) showed a peak DNA synthesis 24 hours after PHx in both

Tab. 1: Basal serum characteristics of the groups.

Serum characteristics	**ST-1**	**ST-1_PHx 24h**	**ST-1_PHx 48h**	**ST-1_PHx 72h**	**HFD**	**HFD_PHx 24h**	**HFD_PHx 48h**	**HFD_PHx 72h**
ALT (µkat/l)	0.7 ± 0.1	**4.6 ± 3.3****	2.2 ± 1.9	1.4 ± 0.4	0.9 ± 0.3	1.8 ± 0.5	1.2 ± 0.4	**2.5 ± 1.1**$^{\#}$
AST (µkat/l)	1.9 ± 0.2	**7.7 ± 2.7****	**4.4 ± 1.7***	2.6 ± 0.5	2.2 ± 0.3	4.9 ± 1.9	3.2 ± 1.4	3.5 ± 1.2
ALP (µkat/l)	2.3 ± 0.4	**5.1 ± 1.8***	**5.3 ± 2.2***	4.0 ± 0.8	2.5 ± 0.4	4.8 ± 1.0	**5.3 ± 1.8**$^{\#}$	**6.9 ± 1.2**$^{\#\#, \$}$
Total bilirubin (µmol/l)	1.8 ± 0.4	6.8 ± 5.0	7.3 ± 6.1	5.7 ± 1.6	1.8 ± 1.0	5.2 ± 1.2	5.3 ± 2.9	**6.0 ± 2.4**$^{\#}$

The values represent the mean ± SD (n = 6). ALT – alanine aminotransferase, AST – aspartate aminotransferase, ALP – alkaline phosphatase, HFD – high fat diet, PHx – partial hepatectomy, ST-1 – standard diet. * $p < 0.05$, ** $p < 0.001$ vs ST-1; $^{\#}$ $p < 0.05$, $^{\#\#}$ $p < 0.001$ vs HFD; $^{\$}$ $p < 0.05$ vs corresponding ST-1 group.

ST-1 and HFD groups ($p < 0.001$) with subsequent gradual decrease in BrdU incorporation (48 h, $p < 0.001$; 72 h $p < 0.001$). There were not differences between ST-1 and HFD group in DNA synthesis after PHx in any corresponding time interval. Nevertheless, zonal distribution of DNA synthesis was more pronounced in HFD groups lacking labeled cells in centrilobular zone.

Liver characteristics

Feeding with HFD induced significant accumulation of TAG ($p < 0.05$) and cholesterol ($p < 0.001$) in the liver (table 2). Accumulation of fat was confirmed by histological findings (oil red staining, data not shown). Although we did not observe inflammatory infiltration in the liver, fatty liver exerted increased markers of oxidative stress. Hepatic amount of GSH was lowered ($p < 0.05$) and MDA content was increased ($p < 0.001$) when compared with non-steatotic controls (table 2). Other liver parameters (absolute and relative liver weights, IL-6, TGF-β1, content of DNA) did not significantly differ between ST-1 and HFD control groups.

Partial hepatectomy led to a significant decrease in absolute and relative liver weights, total and relative DNA contents in non-fatty and steatotic livers. In ST-1 group, PHx induced significant accumulation of TAG in the liver after 24 hours ($p < 0.05$), whereas in HFD, PHx did not lead to additional increase in hepatic content of TAG. Hepatic cholesterol was significantly decreased 24, 48 and 72 hours after PHx only in HFD rats.

Regenerating liver exerted lowering of markers of oxidative stress when compared to corresponding controls.

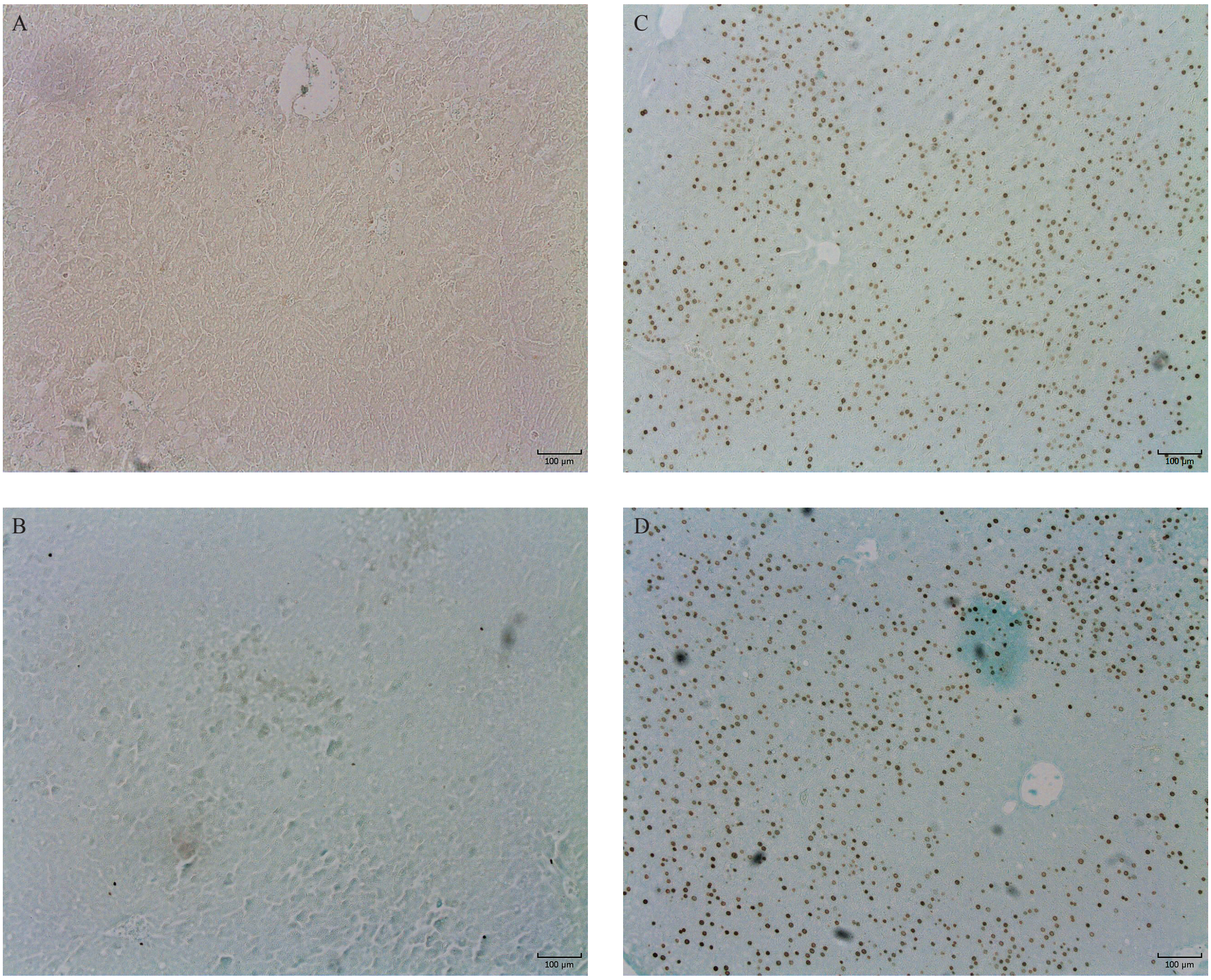

Fig. 1: Immunohistochemistry of BrdU incorporation in the liver. Samples of livers taken from control rats fed with ST-1 diet (1A) or HFD (1B) and from ST-1 (1C) and HFD (1D) animals 24 hours after PHx (ST-1 – control, HFD – high fat diet, PHx – partial hepatectomy). Objective magnification 10×, bar 100 µm.

Tab. 2: Basal liver characteristics of the groups.

Liver characteristics	**ST-1**	**ST-1_PHx 24h**	**ST-1_PHx 48h**	**ST-1_PHx 72h**	**HFD**	**HFD_PHx 24h**	**HFD_PHx 48h**	**HFD_PHx 72h**
Absolute liver weight (g)	11.0 ± 1.2	**5.7 ± 0.7****	6.5 ± 0.7	7.2 ± 0.5	12.0 ± 2.5	**5.2 ± 0.5**$^{\#\#\#}$	7.5 ± 1.5	7.3 ± 1.0
Relative liver weight (% of body weight)	2.5 ± 0.1	**1.3 ± 0.1*****	1.6 ± 0.1	1.8 ± 0.1	2.6 ± 0.2	**1.3 ± 0.1**$^{\#\#\#}$	1.7 ± 0.2	1.9 ± 0.1
Liver triacylgly-cerols (mmol/kg)	7.0 ± 3.9	**50.0 ± 21.9***	28.0 ± 8.2	26.2 ± 9.2	**48.3 ± 20.0***	53.6 ± 18.5	60.4 ± 10.1	53.6 ± 9.7
Liver cholesterol (mmol/kg)	7.1 ± 2.0	9.0 ± 2.6	7.8 ± 0.9	8.2 ± 1.1	**31.8 ± 8.7*****	**19.0 ± 6.6**$^{\#\#\#,\$}$	**20.4 ± 4.9**$^{\#\#,\$\$\$}$	**15.1 ± 3.1**$^{\#\#\#}$
Liver GSH (mmol/kg)	15.1 ± 2.8	**21.6 ± 4.1****	19.0 ± 2.1	17.4 ± 2.5	**9.6 ± 3.6***	**16.6 ± 2.0**$^{\#\#}$	14.6 ± 2.8	**18.6 ± 1.0**$^{\#\#\#}$
GSH/GSSG ratio	9.4 ± 0.8	**10.8 ± 0.8***	**10.7 ± 0.4***	**11.4 ± 0.7*****	9.3 ± 1.0	10.0 ± 0.8	**10.9 ± 0.5**$^{\#}$	**12.8 ± 0.4**$^{\#\#\#,\$}$
Liver MDA (nmol/g liver)	28.2 ± 2.8	18.6 ± 5.3	11.1 ± 6.2	22.6 ± 1.9	**72.1 ± 17.9*****	**30.9 ± 14.0**$^{\#\#\#}$	**36.2 ± 11.8**$^{\#\#\#,\$\$}$	**47.5 ± 11.0**$^{\#\#,\$\$}$
Liver IL-6 (pg/mg protein)	14.6 ± 6.6	20.7 ± 2.0	20.4 ± 6.6	N/A	16.1 ± 4.6	**25.3 ± 2.4 #**	20.8 ± 3.9	N/A
Liver TGF-β1 (pg/mg protein)	15.7 ± 2.7	10.3 ± 1.3	10.6 ± 3.7	17.1 ± 5.6	16.3 ± 6.9	10.3 ± 3.2	10.7 ± 2.5	18.7 ± 5.0
DNA content (mg DNA/g liver)	1.7 ± 0.1	**1.2 ± 0.1***	1.2 ± 0.4	1.7 ± 0.1	1.7 ± 0.1	1.2 ± 0.2	1.5 ± 0.6	1.5 ± 0.2
Total DNA content (mg DNA/liver)	18.6 ± 1.5	**6.8 ± 0.9*****	9.2 ± 3.2	12.5 ± 1.1	18.7 ± 1.8	**6.0 ± 0.8**$^{\#\#\#}$	9.2 ± 1.9	11.2 ± 2.1

The values represent the mean ± SD (n = 6). GSH – reduced form of glutathione, GSSG – oxidized form of glutathione, HFD – high fat diet, IL-6 - interleukin-6, MDA – malondialdehyde, PHx – partial hepatectomy, ST-1 – standard diet, TGF-β1 – transforming growth factor β1. * $p < 0.05$, ** $p < 0.01$, *** $p < 0.001$ vs ST-1; # $p < 0.05$, ## $p < 0.01$, ### $p < 0.001$ vs HFD; \$ $p < 0.05$, \$\$ $p < 0.01$, \$\$\$ $p < 0.001$ vs corresponding ST-1 group.

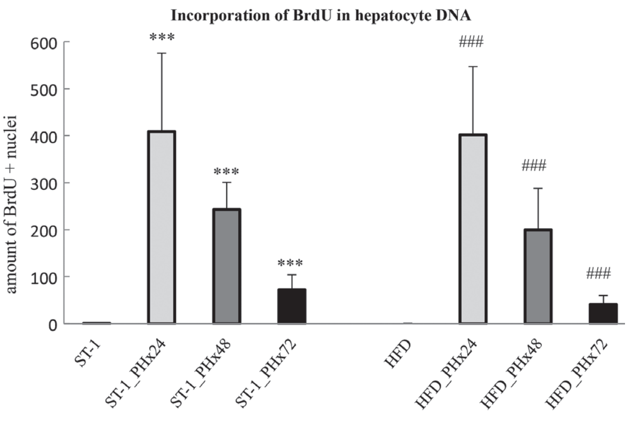

Fig. 2: Quantification of BrdU-positive nuclei in histopathological liver samples of ST-1 and HFD fed animals in 24, 48 and 72 hours after PHx. HFD – high fat diet, PHx – partial hepatectomy, ST-1 – standard diet. *** $p < 0.001$ vs ST-1; ### $p < 0.001$ vs HFD.

Liver GSH was elevated 24 hours after PHx in ST-1 animals ($p < 0.01$) and 24 ($p < 0.01$) and 72 ($p < 0.001$) hours after PHx in HFD rats. Ratio of GSH to GSSG was increased in 24, 48 and 72 hours after PHx in ST-1 groups, and in 48 and 72 h in HFD. Hepatic MDA content was significantly decreased in all measured time intervals after PHx in HFD groups. A non-significant trend of liver MDA reduction after PHx was also observed in ST-1 groups.

An elevation of hepatic IL-6 level was induced by PHx in 24h interval in HFD ($p < 0.05$). A similar, non-significant increase in IL-6 was observed 24 h after PHx in ST-1 group. Liver content of TGB-β1 exerted a non-significant decrease 24 and 48 h after PHx in both ST-1 and HFD groups.

Respiration of mitochondria in liver homogenate

As shown in table 3, respiration of mitochondria in liver homogenate at state 3 showed only a non-significant trend of increased oxygen consumption after addition of substrates of

Tab. 3: Oxygen consumption of mitochondria in liver homogenate at state 3 and RCI.

Respiration	ST-1	ST-1_PHx 24h	ST-1_PHx 48h	ST-1_PHx 72h	HFD	HFD_PHx 24h	HFD_PHx 48h	HFD_PHx 72h
State 3 oxygen consumption at presence of complex I substrates	100.0 ± 23.7	145.0 ± 28.8	167.6 ± 58.7	91.4 ± 18.1	92.1 ± 36.6	160.6 ± 36.5	156.5 ± 19.9	58.4 ± 9.0
State 3 oxygen consumption at presence of complex II substrate	100.0 ± 24.9	104.9 ± 19.0	112.4 ± 33.2	85.0 ± 13.1	102.3 ± 2.4	103.7 ± 29.9	112.8 ± 30.6	100.3 ± 13.0
RCI at presence of complex II substrate	2.9 ± 0.6	5.5 ± 1.1	3.2 ± 0.3	2.1 ± 0.3	4.0 ± 0.6	5.8 ± 0.7	4.5 ± 1.2	2.3 ± 0.2

The values of respiration at state 3 represent the mean ± SD and are expressed in % where 100% is respiration of ST-1 control group. HFD – high fat diet, PHx – partial hepatectomy, RCI – respiratory control index, ST-1 – standard diet. n = 3–4.

respiratory complex I in both ST-1 and HFD groups 24 and 48 hours after PHx. There were not changes in respiration at state 3 of complex II PHx in any group. RCI of complex II showed a non-significant trend of an elevation 24 hours after PHx in both groups.

Discussion

NAFLD is a frequent chronic liver disease and its worldwide prevalence continues to grow with the increasing incidence of obesity. The prevalence of NAFLD in Western countries is 20–30%; about 2–3% of the general population suffers from non-alcoholic steatohepatitis (38). Steatosis is taken as an important risk factor for postoperative complication after major hepatectomy in experimental conditions and in clinical practice (39, 40).

Nevertheless, there are controversial data concerning the course of regeneration of steatotic liver; some authors found impaired regeneration of the liver affected by NAFLD (41, 42) while others did not (25, 43). The reasons of such inconsistency could be explained by different models, various degrees of steatosis and diverse stages of NAFLD used for induction of steatosis. Most of earlier studies were based on genetic leptin mutations (ob/ob mice, Zucker rats) or on methionine- and choline-deficient diet which do not correspond well with the picture of simple steatosis in human.

Therefore we decided to use nutritional model of steatosis which we described in our previous paper (14). In present study feeding rats with HFD for six weeks caused simple microvesicular steatosis without inflammatory reaction or fibrosis. Liver steatosis was confirmed by the triacylglycerol (TAG) content in the liver, which was almost sevenfold greater in HFD group in comparison to control rats. It is commonly known that the transient hepatocellular fat accumulation in the early phase of regeneration following PHx is required for physiological liver regeneration (44). Significantly increased TAG content in the liver 24 hours after PHx in rats fed with ST-1 is in good accordance with previous studies. In contrast to ST-1 fed animals, we did not observe any further changes in hepatic levels of TAG induced by partial hepatectomy in HFD rats.

Cell turnover in normal liver is very low and rate of hepatocyte DNA synthesis represents less than 0.1%. It is generally accepted that homeostatic liver renewal arises by replication of pre-existing hepatocytes rather than stem cell differentiation (45). It was repeatedly documented using [^{3}H]-thymidine incorporation that the first hepatocytes to divide after PHx are periportal with the peak of DNA synthesis 18–20 hours after surgery (46, 47); DNA synthesis in centrilobular area is delayed by about 10 hours. BrdU labelling, widely used as a marker of proliferating hepatocytes, correlates well with the use of [^{3}H]-thymidine (48). Our results of significant increase of BrdU incorporation after PHx in control rats is in good concordance with findings of others (1, 46, 47, 49). Proliferative response in rats with simple steatosis was not altered in comparison to controls. The only difference was more pronounced zonal distribution of labelled hepatocytes with almost lacking cells in centrilobular zone in HFD rats. This could be explained by delayed onset of regenerative response as result from zonal kinetics of hepatocyte proliferation. Centrilobular zone has the poorest oxygen supply and the lack of oxygen can be further potentiated by high-fat diet in this zone (13). In accordance with our results Vetelainen and co-workers have shown that mild steatosis induced by a methionine- and choline-deficient diet did not affect liver regeneration after PHx; however, mild steatosis impaired functional recovery and increased hepatocellular damage after liver resection (21). Interleukin-6

(IL-6) has been shown to play an important role in initiating liver regeneration via activating signal transducer and activator of transcription 3 (STAT3). The role of IL-6 dependent signalling during liver regeneration is attributed mainly to induction of acute phase response; serum levels of IL-6 in rats are elevated during the first hours after PHx preceding by hours increase of liver DNA synthesis (50). We found a trend of increasing liver IL-6 concentration after PHx in both control and HFD groups. Transforming growth factor beta1 (TGF-β1) signalling pathway exerts an antiproliferative effect on hepatocytes. It has been documented that TGF-β1 reversibly inhibits proliferative response after PHx and its signalling is inhibited in the early phase of liver regeneration (51). Our results fit their findings since we observed transient decrease of hepatic TGF-β1content 24 and 48 hours after PHx in both groups.

Impaired redox balance and oxidative stress belong to critical mechanisms in the pathogenesis of NAFLD (52). In accordance with this, we found that feeding with HFD caused induction of hepatic oxidative stress as documented by decreased content of GSH and increased concentration of MDA in steatotic liver. Partial hepatectomy attenuated level of lipoperoxidation and elevated content of GSH in steatotic liver. Similar effect was also observed in ST-1 fed rats. The increase in hepatic GSH after PHx corresponds to previous observations of Riehle and Huang (53, 54) who concluded that GSH is required for normal course of liver regeneration. An increase in GSH in the regenerating liver is necessary for hepatocyte entering the S phase (54). Moreover, mice deficient in GSH synthesis have also impaired priming, delayed DNA synthesis and low level apoptosis after PHx (53). Although we did not observe any significant difference in BrdU labelling after PHx in steatotic livers, the potential delay in S phase in these livers (absence of BrdU staining in pericentral area 24 hours after PHx in fatty livers) could be caused by significantly lower GSH content. Nevertheless, fatty livers maintain ability to increase hepatic level of GSH in response to liver resection which may explain no difference in DNA synthesis between steatotic and non-fatty livers after PHx. An increase of GSH during regeneration corresponds to a decrease in lipid peroxidation in both fatty and non-steatotic livers.

Mitochondrial dysfunction plays an important role in the development of NAFLD (12). Moreover, increased mitochondrial production of ROS may participate on impaired redox balance in NAFLD. Although many authors proofed changes in the function of mitochondria in NAFLD (12, 19, 20, 55), we did not observe significant differences in RCI for complex II and in state 3 respirations in the presence of complex I or II substrates between ST-1 and HFD. PHx did not induce any significant changes in respiration in any group. However, oxygen consumption at state 3 in the presence of complex I substrates showed a trend of transient increasing respiration 24 and 48 hours after PHx in both lean and steatotic groups. Such increase in respiration at state 3 after PHx was not detected when complex II substrate was used which corresponds with findings of Yang (56). We also observed a trend of transient increase in RCI at presence of complex II substrate in both groups 24 h after PHx which is in accordance with literature (56).

In summary, 2/3 partial hepatectomy-induced regeneration of the rat liver with simple microvesicular steatosis was not significantly affected when compared to the lean liver.

Acknowledgements

This study was supported by PRVOUK P37/02 and SVV 260287.

References

1. Bucher NL, Swaffield MN. The rate of incorporation of labelled thymidine into the deoxyribonucleic acid of regenerating rat liver in relation to the amount of liver excised. Cancer Res 1964; 24: 1611–25.
2. Michalopoulos GK, DeFrances MC. Liver regeneration. Science 1997; 276: 60–6.
3. Higgins G, Anderson R. Experimental pathology of the liver. I. Restoration of the liver of the white rat following partial surgical removal. Archives of pathology (Chic) 1931; 12: 186–202.
4. Fausto N. Liver regeneration. J Hepatol 2000; 32: 19–31.
5. Fausto N, Campbell JS, Riehle KJ. Liver regeneration. Hepatology 2006; 43: S45–53.
6. Mangnall D, Bird NC, Majeed AW. The molecular physiology of liver regeneration following partial hepatectomy. Liver Int 2003; 23: 124–38.
7. Rychtrmoc D, Hubalkova L, Viskova A, Libra A, Buncek M, Cervinkova Z. Transcriptome temporal and functional analysis of liver regeneration termination. Physiol Res 2012; 61 Suppl 2: S77–92.
8. Trevisani F, Colantoni A, Caraceni P, Van Thiel DH. The use of donor fatty liver for liver transplantation: a challenge or a quagmire? J Hepatol 1996; 24: 114–21.
9. Behrns KE, Tsiotos GG, DeSouza NF, Krishna MK, Ludwig J, Nagorney DM. Hepatic steatosis as a potential risk factor for major hepatic resection. J Gastrointest Surg 1998; 2: 292–8.
10. Erickson SK. Nonalcoholic fatty liver disease. J Lipid Res 2009; 50 Suppl: S412–6.
11. Chalasani N, Younossi Z, Lavine JE, et al. The diagnosis and management of nonalcoholic fatty liver disease: Practice guideline by the American Association for the Study of Liver Diseases, American College of Gastroenterology, and the American Gastroenterological Association. Am J Gastroenterol 2012; 107: 811–26.
12. Vendemiale G, Grattagliano I, Caraceni P, et al. Mitochondrial oxidative injury and energy metabolism alteration in rat fatty liver: effect of the nutritional status. Hepatology 2001; 33: 808–15.
13. Mantena SK, Vaughn DP, Andringa KK, et al. High fat diet induces dysregulation of hepatic oxygen gradients and mitochondrial function in vivo. Biochem J 2009; 417: 183–93.
14. Kucera O, Garnol T, Lotkova H, et al. The effect of rat strain, diet composition and feeding period on the development of a nutritional model of non-alcoholic fatty liver disease in rats. Physiol Res 2011; 60: 317–28.
15. Paradies G, Paradies V, Ruggiero FM, Petrosillo G. Oxidative stress, cardiolipin and mitochondrial dysfunction in nonalcoholic fatty liver disease. World J Gastroenterol 2014; 20: 14205–18.
16. Sanyal AJ, Campbell-Sargent C, Mirshahi F, et al. Nonalcoholic steatohepatitis: association of insulin resistance and mitochondrial abnormalities. Gastroenterology 2001; 120: 1183–92.
17. Kawahara H, Fukura M, Tsuchishima M, Takase S. Mutation of mitochondrial DNA in livers from patients with alcoholic hepatitis and nonalcoholic steatohepatitis. Alcohol Clin Exp Res 2007; 31: S54–60.
18. Gao D, Wei C, Chen L, Huang J, Yang S, Diehl AM. Oxidative DNA damage and DNA repair enzyme expression are inversely related in murine models of fatty liver disease. Am J Physiol Gastrointest Liver Physiol 2004; 287: G1070–7.
19. Perez-Carreras M, Del Hoyo P, Martin MA, et al. Defective hepatic mitochondrial respiratory chain in patients with nonalcoholic steatohepatitis. Hepatology 2003; 38: 999–1007.
20. Garcia-Ruiz I, Rodriguez-Juan C, Diaz-Sanjuan T, et al. Uric acid and anti-TNF antibody improve mitochondrial dysfunction in ob/ob mice. Hepatology 2006; 44: 581–91.
21. Vetelainen R, Bennink RJ, van Vliet AK, van Gulik TM. Mild steatosis impairs functional recovery after liver resection in an experimental model. Br J Surg 2007; 94: 1002–8.
22. Selzner M, Clavien PA. Failure of regeneration of the steatotic rat liver: disruption at two different levels in the regeneration pathway. Hepatology 2000; 31: 35–42.

23. Kele PG, van der Jagt EJ, Gouw AS, Lisman T, Porte RJ, de Boer MT. The impact of hepatic steatosis on liver regeneration after partial hepatectomy. Liver Int 2013; 33: 469–75.
24. de Meijer VE, Kalish BT, Puder M, Ijzermans JN. Systematic review and meta-analysis of steatosis as a risk factor in major hepatic resection. Br J Surg 2010; 97: 1331–9.
25. Picard C, Lambotte L, Starkel P, et al. Steatosis is not sufficient to cause an impaired regenerative response after partial hepatectomy in rats. J Hepatol 2002; 36: 645–52.
26. Sydor S, Gu Y, Schlattjan M, et al. Steatosis does not impair liver regeneration after partial hepatectomy. Lab Invest 2013; 93: 20–30.
27. Cho JY, Suh KS, Kwon CH, Yi NJ, Lee KU. Mild hepatic steatosis is not a major risk factor for hepatectomy and regenerative power is not impaired. Surgery 2006; 139: 508–15.
28. Lieber CS, Leo MA, Mak KM, et al. Model of nonalcoholic steatohepatitis. Am J Clin Nutr 2004; 79: 502–9.
29. Drahota Z, Palenickova E, Endlicher R, et al. Biguanides inhibit complex I, II and IV of rat liver mitochondria and modify their functional properties. Physiol Res 2014; 63: 1–11.
30. Cervinkova Z, Kucera O, Lotkova H, Drahota Z, Houstek J. [Oxygraphic evaluation of energy metabolism in isolated hepatocytes]. Acta Medica (Hradec Kralove) Suppl 2002; 45: 65–76.
31. Hissin PJ, Hilf R. A fluorometric method for determination of oxidized and reduced glutathione in tissues. Analytical biochemistry 1976; 74: 214–26.
32. Rousar T, Kucera O, Lotkova H, Cervinkova Z. Assessment of reduced glutathione: comparison of an optimized fluorometric assay with enzymatic recycling method. Anal Biochem 2012; 423: 236–40.
33. Bligh EG, Dyer WJ. A rapid method of total lipid extraction and purification. Can J Biochem Physiol 1959; 37: 911–7.
34. Burton K. A study of the conditions and mechanism of the diphenylamine reaction for the colorimetric estimation of deoxyribonucleic acid. Biochem J 1956; 62: 315–23.
35. Bradford MM. A rapid and sensitive method for the quantitation of microgram quantities of protein utilizing the principle of protein-dye binding. Anal Biochem 1976; 72: 248–54.
36. Pilz J, Meineke I, Gleiter CH. Measurement of free and bound malondialdehyde in plasma by high-performance liquid chromatography as the 2,4-dinitrophenylhydrazine derivative. J Chromatogr B Biomed Sci Appl 2000; 742: 315–25.
37. Bader A, Pavlica S, Deiwick A, et al. Proteomic analysis to display the effect of low doses of erythropoietin on rat liver regeneration. Life Sci 2011; 89: 827–33.
38. Bellentani S, Scaglioni F, Marino M, Bedogni G. Epidemiology of non-alcoholic fatty liver disease. Dig Dis 2010; 28: 155–61.
39. McCormack L, Petrowsky H, Jochum W, Furrer K, Clavien PA. Hepatic steatosis is a risk factor for postoperative complications after major hepatectomy: a matched case-control study. Ann Surg 2007; 245: 923–30.
40. Vetelainen R, van Vliet AK, van Gulik TM. Severe steatosis increases hepatocellular injury and impairs liver regeneration in a rat model of partial hepatectomy. Ann Surg. 2007; 245: 44–50.
41. Murata H, Yagi T, Iwagaki H, et al. Mechanism of impaired regeneration of fatty liver in mouse partial hepatectomy model. J Gastroenterol Hepatol 2007; 22: 2173–80.
42. DeAngelis RA, Markiewski MM, Taub R, Lambris JD. A high-fat diet impairs liver regeneration in C57BL/6 mice through overexpression of the NF-kappaB inhibitor, IkappaBalpha. Hepatology 2005; 42: 1148–57.
43. Rao MS, Papreddy K, Abecassis M, Hashimoto T. Regeneration of liver with marked fatty change following partial hepatectomy in rats. Dig Dis Sci 2001; 46: 1821–6.
44. Rudnick DA, Davidson NO. Functional Relationships between Lipid Metabolism and Liver Regeneration. Int J Hepatol 2012; 2012: 549241.
45. Yanger K, Knigin D, Zong Y, et al. Adult hepatocytes are generated by self-duplication rather than stem cell differentiation. Cell Stem Cell 2014; 15: 340–9.
46. Fabrikant JI. The kinetics of cellular proliferation in regenerating liver. J Cell Biol 1968; 36: 551–65.
47. Grisham JW. A morphologic study of deoxyribonucleic acid synthesis and cell proliferation in regenerating rat liver; autoradiography with thymidine-H3. Cancer Res 1962; 22: 842–9.
48. Yu CC, Woods AL, Levison DA. The assessment of cellular proliferation by immunohistochemistry: a review of currently available methods and their applications. Histochem J 1992; 24: 121–31.
49. Weglarz TC, Sandgren EP. Timing of hepatocyte entry into DNA synthesis after partial hepatectomy is cell autonomous. Proc Natl Acad Sci U S A. 2000; 97: 12595–600.
50. Streetz KL, Luedde T, Manns MP, Trautwein C. Interleukin 6 and liver regeneration. Gut 2000; 47: 309–12.
51. Russell WE, Coffey RJ, Jr., Ouellette AJ, Moses HL. Type beta transforming growth factor reversibly inhibits the early proliferative response to partial hepatectomy in the rat. Proc Natl Acad Sci U S A 1988; 85: 5126–30.
52. Gambino R, Musso G, Cassader M. Redox balance in the pathogenesis of nonalcoholic fatty liver disease: mechanisms and therapeutic opportunities. Antioxid Redox Signal 2011; 15: 1325–65.
53. Riehle KJ, Haque J, McMahan RS, Kavanagh TJ, Fausto N, Campbell JS. Sustained Glutathione Deficiency Interferes with the Liver Response to TNF-alpha and Liver Regeneration after Partial Hepatectomy in Mice. J Liver Disease Transplant 2013; 1.
54. Huang ZZ, Li H, Cai J, Kuhlenkamp J, Kaplowitz N, Lu SC. Changes in glutathione homeostasis during liver regeneration in the rat. Hepatology 1998; 27: 147–53.
55. Cortez-Pinto H, Chatham J, Chacko VP, Arnold C, Rashid A, Diehl AM. Alterations in liver ATP homeostasis in human nonalcoholic steatohepatitis: a pilot study. JAMA 1999; 282: 1659–64.
56. Yang S, Tan TM, Wee A, Leow CK. Mitochondrial respiratory function and antioxidant capacity in normal and cirrhotic livers following partial hepatectomy. Cell Mol Life Sci 2004; 61: 220–9.

Received: 23/05/2016
Accepted: 06/06/2016

ORIGINAL ARTICLE

Association of Atrial Fibrillation with Morphological and Electrophysiological Changes of the Atrial Myocardium

Adéla Matějková[*], *Ivo Šteiner*

Charles University, Faculty of Medicine and University Hospital in Hradec Králové, Czech Republic: Fingerland Department of Pathology
* Corresponding author: Fingerland Department of Pathology, Charles University, Faculty of Medicine and Faculty Hospital in Hradec Králové, Sokolská 581, 500 05 Hradec Králové, Czech Republic; email: adela.matejkova@gmail.com

Summary: Atrial fibrillation (AF) is the most common sustained cardiac arrhythmia. For long time it was considered as pure functional disorder, but in recent years, there were identified atrial locations, which are involved in the initiation and maintenance of this arrhythmia. These structural changes, so called remodelation, start at electric level and later they affect contractility and morphology. In this study we attempted to find a possible relation between morphological (scarring, amyloidosis, left atrial (LA) enlargement) and electrophysiological (ECG features) changes in patients with AF. We examined grossly and histologically 100 hearts of necropsy patients – 54 with a history of AF and 46 without AF. Premortem ECGs were evaluated. The patients with AF had significantly heavier heart, larger LA, more severely scarred myocardium of the LA and atrial septum, and more severe amyloidosis in both atria. Severity of amyloidosis was higher in LAs vs. right atria (RAs). Distribution of both fibrosis and amyloidosis was irregular. The most affected area was in the LA anterior wall. Patients with a history of AF and with most severe amyloidosis have more often abnormally long P waves. Finding of long P wave may contribute to diagnosis of a hitherto undisclosed atrial fibrillation.

Keywords: *Atrial fibrillation; Isolated atrial amyloid; Myocardial scarring; Electrocardiographic features; P wave*

Introduction

Atrial fibrillation (AF) is the most common sustained cardiac arrhythmia in the group of supraventricular arrhythmias (7, 11). Although it does not directly endanger the patient's life, it certainly cannot be regarded as benign. In the Czech Republic, AF is the commonest arrhythmia leading to hospitalization (16). There are several complications associated with AF, particularly thromboembolism, more common heart failure and poorer quality of life. Patients with AF have markedly increased mortality. In developed countries, the prevalence of AF is 1–2% (11). With ageing, its prevalence significantly rises. In the fifth decennium it is 1% and doubles in each sequential decennium, reaching more than 10% in octogenerians (7, 16). For subjects aged 40+ years, regardless of gender, the risk of AF is estimated at 25% (15).

AF is a complex arrhythmia. It affects a wide spectrum of individuals, both with and without structural heart diseases. The key risk factors for AF include, in addition to age, arterial hypertension, congestive heart failure and valvular diseases (7). In AF, the heart rhythm is not controlled by the sinoatrial node, but by multiple ectopic pacemakers in the atrial chambers, resulting in chaotic depolarization of atrial myocardium, which eventually becomes sustained by local reentrant circuits. The most common site for triggering premature atrial contraction are foci in atrial walls, particularly in so called myocardial sleeves of pulmonary veins (7, 9, 10).

The key etiopathogenic factor of AF seems to be restructuring (remodelation) of the atrial myocardium leading to atrial conduction abnormalities. This remodelation starts at electric level and later it affects contractility and structure (1). The structural changes are both geometric – dilatation of the atria, and anatomo-histological – fibrosis and amyloidosis of atrial myocardium, particularly deposition of isolated atrial amyloid (IAA). The incidence of both AF and IAA is related to ageing (2, 7, 21). The dominant heart chamber for development of AF is the left atrium (LA); the right atrium (RA) plays a minor role. There exists a vicious circle – the once developed AF is self-worsening, as it leads to more structural rebuilding of the atrial myocardium and this is associated with progression of AF into its more sustained forms (19).

In this study, in cooperation with clinicians-cardiologists, we attempted to find possible relation between morphological changes of atrial myocardium and electrophysiological (ECG) abnormalities of atrial conduction, by comparing two groups of necropsy patients – those with AF and those without AF (control group). Particular attention was paid to cases with heavy amyloid infiltration of the atrial myocardium.

http://dx.doi.org/10.14712/18059694.2016.88

Material and Methods

During 2007–2011 we examined 100 hearts of patients autopsied at the Fingerland Department of Pathology in Hradec Králové. The criteria required for inclusion in the study were patient's age 50–90 years, and an available ECG record from less than 3 months before death. The study was approved by the Ethical Committee of Faculty Hospital in Hradec Králové.

The total of 100 patients studied comprised two main groups – **AF group** – 54 patients with a history of AF, and **SINUS group** – 46 patients with a proved sinus rhythm. The groups were age- and sex-matched. The AF group was further subclassified into two subgroups: subgroup AFF – patients with AF present on their last ECG, and subgroup AFS – patients with a history of AF who, however, had sinus rhythm on their last ECG. Information regarding the type of AF was retrospectively obtained from the patient's clinical documentation. The **subgroup AFF** (n = 25) comprised patients with the following types of AF: 2 newly diagnosed, 2 paroxysmal, 4 persistent, 5 permanent, 7 described as "chronic", and 5 not specified. Analogically, the **subgroup AFS** (n = 29) comprised patients with 6 newly diagnosed, 15 paroxysmal, 3 permanent, 3 described as "chronic", and 2 not specified type of AF.

At gross examination of the formalin-fixed hearts attention was paid particularly to the LA. Its interior was measured in 3 dimensions and its volume calculated. Further, we related the LA volume to the patient's body surface area (BSA) by the Du Bois formula: BSA = (body weight$^{0.425}$ × height$^{0.725}$) × 0.007184. This calculation is used in ultrasound examination of the heart to assess the LA size (17).

For histological examination, we obtained five samples from standard sites: RA, 3 samples from the LA – anterior wall (LAA), roof (LAR), and posterior wall (LAP), and interatrial septum (IAS). All samples were processed in a standard way and sections stained by haematoxylin and eosin, by Sirius red (Maldyk) for amyloid, and by Elastica – Van Gieson for fibrous scarring. The degree of IAA deposition in the atrial walls was semiquantitatively graded for each heart on a 0–3 scale according to the following criteria: grade 0 = not present or only small deposits; grade 1 = occasional fine fibers surrounding cardiomyocytes and/or deposited in the walls of small intramyocardial vessels; grade 2 = moderate deposits in the entire thickness of the myocardium; grade 3 = dense network of fibers and/or solid foci of amyloid.

Similarly, the degree of fibrosis (scarring) was assessed: grade 0 = absence or focal loose interstitial fibrosis; grade 1 = mild diffuse interstitial fibrosis or few small solid foci; grade 2 = moderate degree of interstitial fibrosis or more solid foci in the entire thickness of the myocardium; grade 3 = severe interstitial fibrosis or large solid foci.

The patient's baseline 12 – lead ECGs, obtained in the supine position usually just prior to death with 25 mm/s and 10 mm/mV standardization, were screened by Vignendra Ariyarajah, MD (Saint Boniface Hospital, Winnipeg, Man., Canada) and Jiří Nový, MD (Hospital in Jičín, Faculty Hospital in Hradec Králové). ECGs were assessed with a calibrated, magnifying graticule, in the same way as in the previous study of Ariyarajah et al. (2). The following parameters were assessed: P wave duration (P max, P min), P wave dispersion (P disp – difference in duration between the widest (maximum) and the narrowest (minimum) P wave), P wave axis (P axis), duration of QRS complex (QRS max, QRS min), QRS complex dispersion (QRS disp – difference between the widest and the narrowest QRS complex), and the heart electric axis (QRS axis).

All the results (gross LA parameters, grades of fibrosis and of amyloid deposition) were compared in the AF vs. SINUS groups, and also in both AF subgroups – AFF and AFS vs. SINUS, and AFF vs. AFS.

For evaluation of influence of the myocardial structural changes, particularly the infiltration by IAA on atrial conduction, we compared ECG findings of the group IAA grade 0

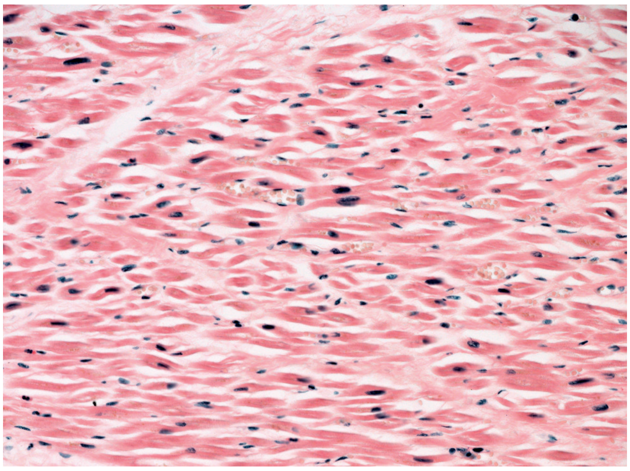

Fig. 1: Sirious red staining of left atrial anterior wall showing IAA grade 0 (amyloid is not present). Magnificantion 200×.

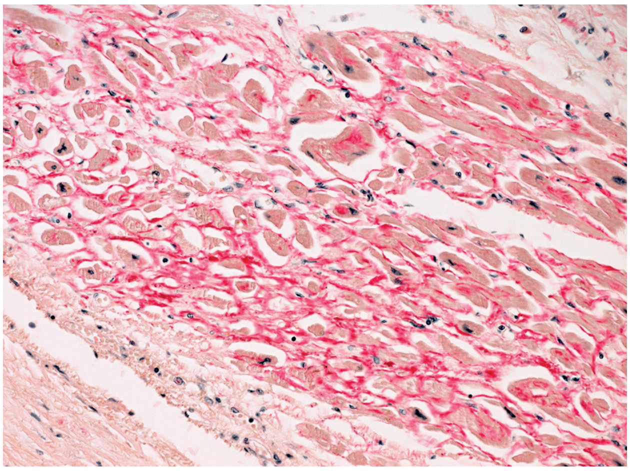

Fig. 2: Sirious red staining of left atrial anterior wall showing IAA grade 3 (dense network of amyloid fibers). Magnificantion 200×.

(fig. 1) with those of IAA grade 3 (fig. 2). (To increase specificity, the IAA groups 1 and 2 were omitted.) For this comparison we used samples from LAA. (In our previous study, this showed significantly most intense infiltration by amyloid (18).) In control cases with sinus rhythm we evaluated features of both P wave and QRS complex. In cases with AF, only QRS complex was evaluated.

The data obtained were evaluated statistically by multiple appropriate tests: two – sample t test, Mann – Whitney's U test, Fisher's LSD Multiple-Comparison Test, Kruskal-Wallis Multiple-Comparison Z-Value Test (Dunn's Test), Fisher's exact test or chi-square test of independence in contingency tables. Quantitative parameters were presented by median with 95% confidence interval. A value of $p \leq 0.05$ was considered to be statistically significant.

Results

Our series of 100 subjects comprised 51 men and 49 women. In the main AF group (54 subjects), there were 29 men and 25 women, with median of age 75 (70–77) years; in the control group SINUS (46 subjects), there were 22 men and 24 women, with median of age 66 (62–74) years. The AF subgroups AFF and AFS comprised 25 subjects (13 men and 12 women) with median of age 74 (69–76) years, and 29 subjects (16 men and 13 women) with median of age 76 (68–80) years, respectively. Baseline characteristics of the groups obtainable at the time of autopsy (age, gender, presence of systemic hypertension, diabetes mellitus, coronary artery disease, mitral stenosis or artificial heart valves) are presented in table 1. Hypertension, diabetes mellitus and mitral valve disease occurred more frequently in patients with AF. Statistically significant difference between groups was obvious only in age ($p = 0.03$) and systemic hypertension ($p = 0.01$).

There were significant differences ($p < 0.001$) in heart weight between the AF and control group; in the AFs the median heart weight was 525 g (480–590 g), while in controls 420 g (390–490 g). Also comparison of the two AF subgroups (AFF, AFS) with the control group showed statistically significant differences ($p < 0.001$). This was most marked with the AFF where the median heart weight was 560 g (470–680 g).

Statistically significant difference between the two main groups ($p = 0.002$) was noted in the LA volume related to body surface; subjects with AF had more voluminous LA: median 87 (79–101) ml than those with sinus rhythm: median 66 (60–76) ml. The same applied to the subgroups AFF and AFS vs. SINUS ($p = 0.004$). The most significant difference was between AFF: median 92 (79–114) ml and controls.

Histological examination showed significantly more severe myocardial fibrosis in all samples of LA walls and interatrial septum in the AF group when compared to controls. In the RA, however, the difference was not statistically significant. Most severe scarring was observed in the AFF subgroup (tab. 2a).

Similar differences were noted in the degree of myocardial deposition of amyloid. More severe amyloidosis was observed in the AF than in the SINUS group, with the AFF subgroup most affected (tab. 2b).

In all groups the severity of amyloid deposits was higher in the LA compared to the RA. In majority of the evaluated areas the difference was statistically significant, except for two comparisons, however, even there the difference was obvious (tab. 3).

Tab. 1: Baseline characteristics of the groups.

	SINUS (n = 46)	AF (n = 54)	AFS (n = 29)	AFF (n = 25)	p value
Age (median with 95% confidence interval), years	66 (62–74)	75 (70–77)	76 (68–80)	74 (69–76)	0.03*
Gender – Male/Female	22/24	29/25	16/13	13/12	0.82
Systemic hypertension	32 (70)	50 (93)	26 (90)	24 (96)	0.01*
Diabetes mellitus	16 (35)	24 (44)	12 (41)	12 (48)	0.55
Coronary artery disease[1]					0.42
≤ 25%	19 (41)	11 (20)	6 (21)	5 (20)	
26–50%	8 (17)	15 (28)	9 (31)	6 (24)	
51–75%	4 (9)	9 (17)	5 (17)	4 (16)	
> 75 %	15 (33)	19 (35)	9 (31)	10 (40)	
Mitral stenosis	6 (13)	10 (19)	7 (24)	3 (12)	–
Artificial mitral valve	0 (0)	3 (6)	3 (10)	0 (0)	–

All values represent numbers of patients with percentages in parentheses unless indicated otherwise.
n = number of hearts in individual group or subgroup. [1] Degree of atherosclerotic luminal stenosis at autopsy.
* $p \leq 0.05$ considered as significant difference.

Tab. 2: Two – sample and three – sample comparison of atrial myocardial structural changes.

a) Severity of scarring in particular areas of the atria.

SCARRING	AF (n = 54)	SINUS (n = 46)	*p*	AFS (n = 29)	AFF (n = 25)	SINUS (n = 46)	*p*
RA	1.46	1.46	*n.s.*	1.62	1.28	1.46	*n.s.*
LAA	1.72	1.11	*0.004*	1.55	1.92	1.11	*0.010*
LAR	1.70	1.04	*< 0.001*	1.48	1.96	1.04	*< 0.001*
LAP	1.59	1.15	*0.001*	1.45	1.76	1.15	*0.001*
IAS right	1.26	0.74	*0.001*	1.21	1.32	0.74	*0.003*
IAS left	1.63	1.07	*0.010*	1.45	1.84	1.07	*0.006*

b) Severity of amyloid infiltration in particular areas of the atria.

AMYLOID	AF (n = 54)	SINUS (n = 46)	*p*	AFS (n = 29)	AFF (n = 25)	SINUS (n = 46)	*p*
RA	1.56	0.98	*0.002*	1.34	1.80	0.98	*0.001*
LAA	2.39	1.59	*0.005*	2.31	2.48	1.59	*0.030*
LAR	1.77	1.22	*0.007*	1.72	1.83	1.22	*0.052*
LAP	2.02	1.22	*0.003*	2.00	2.04	1.22	*0.023*
IAS right	0.70	0.50	*0.003*	0.69	0.72	0.50	*0.003*
IAS left	1.96	1.48	*0.010*	1.97	1.96	1.48	*n.s.*

The tables show average grades of scarring and amyloid infiltration in the heart atria. For statistical evaluation, the Fisher's exact test and chi-square test of independence in contingency tables were used. A value of $p \leq 0.05$ was considered to be statistically significant. n = number of hearts; n.s. = no significant difference.

Tab. 3: Comparison of right vs. left atrial amyloidosis in individual groups.

AMYLOID	RA	LAA	*p*	IAS right	IAS left	*p*
SINUS (n = 46)	0.98	1.59	*0.001*	0.50	1.48	*< 0.001*
AF (n = 54)	1.56	2.39	*0.003*	0.70	1.96	*< 0.001*
AFS (n = 29)	1.34	2.31	*n.s.*	0.69	1.97	*< 0.001*
AFF (n = 25)	1.80	2.48	*0.050*	0.72	1.96	*n.s.*

The table shows average grades of amyloidosis in particular areas of heart atria. For statistical evaluation, the Fisher's exact test and chi-square test of independence in contingency tables were used. A value of $p \leq 0.05$ was considered to be statistically significant. n = number of hearts; n.s. = no significant difference.

The severity of both myocardial fibrosis and amyloidosis was compared in the three systematically examined sites of the left atrium (LAA, LAP and LAR). While severity of fibrosis was not significantly different, amyloidosis showed statistically significant differences ($p < 0.025$–0.001) in all groups (AF, SINUS, AFF and AFS) – it was most intense in the LA anterior wall, followed by LA posterior wall and the roof of the LA.

To check possible impact of structural changes of atrial myocardium on its conduction properties we compared ECG characteristics of the group with no amyloid (grade 0) with the one with most severe amyloidosis (grade 3). Thus, we evaluated 62 ECG records (16 with IAA grade 0 and 46 with IAA grade 3). Of the total 62 cases, 39 featured sinus rhythm, and 23 AF. There was no statistically significant difference in any of the parameters followed between AF and the control group (tab. 4). Further, we examined frequency of the abnormally long P waves (Pmax ≥ 120 ms) between the groups IAA 0 and IAA 3. Long P waves were seen mostly in the IAA 3 group. When comparing this parameter in the subgroup AFS and the controls, long P waves were clearly more common in subjects with history of AF (46% vs. 14%) (tab. 5).

Discussion

Currently, it is generally accepted that AF has a morphological basis and is associated with remodelation of the atrial myocardium (1, 21, 23). This remodelation is based on myocardial injury of various pathogenesis. The two main

Tab. 4: Comparison of ECG features in IAA 0 vs. IAA 3.

P wave	IAA 0 (n = 12)	IAA 3 (n = 27)	p
P max (ms)	100 (90;120)	100 (80;120)	*0.459*
P min (ms)	55 (40;80)	60 (50;70)	*0.836*
P disp (ms)	40 (30;50)	40 (30;50)	*0.356*
P axis (°)	50 (30;70)	50 (45;70)	*0.417*
QRS complex	**IAA 0 (n = 16)**	**IAA 3 (n = 46)**	***p***
QRS max (ms)	105 (90;120)	100 (90;100)	*0.682*
QRS min (ms)	65 (50;80)	70 (60;80)	*0.490*
QRS disp (ms)	40 (30;50)	30 (20;30)	*0.067*
QRS axis (°)	25 (−40;60)	0 (−5;20)	*0.442*

The tables show median values of ECG characteristics with a 95% confidence interval. A value of $p \leq 0.05$ was considered to be statistically significant. n = number of hearts.

Tab. 5: Comparison of "long P wave" frequency in IAA 0 vs. IAA 3, and in AFS vs. SINUS.

P max ≥ 120 (ms)	IAA 0 (n = 12)	IAA 3 (n = 26)
Total (12/38)	3 (25)	9 (35)
AFS (9/19)	1	8
SINUS (3/19)	2	1
	AFS (n = 26)	**SINUS (n = 31)**
P max ≥ 120 (ms)	12 (46)	4 (14)

The values given show numbers of cases with "long P wave" (with percentages in parentheses). n = number of hearts of particular group with evaluable ECGs. Disregarded were patients with either artificial heart rhythm, or recent myocardial infarction.

key factors capable of modifying myocardial structure and function in AF seem to be atrial tachycardia with a high rate of cell depolarization, and volume/pressure overload of LA leading to increased atrial wall stretch (3, 4). These factors are probably responsible for early electrophysiological changes which often precede frank clinical manifestation of AF. In the affected myocardium, the changes are not only electrophysiological but also contractile and particularly structural (1).

These atrial depolarization abnormalities based on atrial myocardial restructuring appear as an arrhythmogenic substrate for development and eventually sustaining of AF. And AF, once established, becomes progressive. It induces further structural changes and worsens the accompanying heart diseases (arterial hypertension, valvular diseases, heart failure etc.), leading to further progression of atrial myocardial injury. This vicious circle is responsible for progression of paroxysmal AF into its more progressive forms (4, 22).

The most frequently cited structural change of atrial myocardium is interstitial fibrosis which interferes with atrial conduction (1, 4, 21). The fibrosis is more or less irreversible, and it seems that the only way how to effectively prevent its formation or progression is antiarrhythmic treatment of AF and treatment of the accompanying heart diseases.

In accordance with findings presented in recent review article by Corradi (4), we showed that patients with AF have significantly more advanced fibrosis in the LA and atrial septum than controls. This, however, did not apply for the RA, where there was no difference in fibrosis between AF and controls. Most severe fibrosis was present in the AFF subgroup, i.e. in patients mostly with a long history of AF, recorded also on the last ECG. This finding is in accordance with results of papers by Kuppahally et al. (13) and by Platonov et al. (20) assessing degree of left atrial myocardial fibrosis in patients with a long history of AF. The former study was based on non-invasive diagnostics by MRI, the latter, like our study, on necropsy histology. Interestingly, Platonov state that in their cohort of patients who died of cardiovascular causes, the extent of fibrosis was not associated with age, but was significantly correlated with AF presence, severity, and duration. They suggest that age-related increase in fibrosis extent does not reach the magnitude of changes observed in AF and age-related changes per se are unlikely to be the sole cause of advanced fibrosis underlying AF.

Another structural change related to development and sustaining of AF is atrial myocardial amyloidosis, in particular the isolated atrial type (IAA). Its precursor – atrial natriuretic peptide (ANP) is normally present in the atrial myocardial interstitium (4).

In our study, we showed that patients with AF, compared to controls, had significantly more severe amyloidosis at all the sites examined. The most severe degree was found in the AFF subgroup. Similar finding was made by Röcken et al., who examined right atrial appendages resected during cardiac surgery (21).

Distribution of amyloid deposits in the atrial walls was irregular, with statistically significant differences. The order of severity was LAA–LAP–LAR. This findings corresponds with that of Šteiner et al. (23), who showed in a study of 100 necropsy patients most severe amyloidosis in the LA anterior wall, particularly in patients with a history of AF. In our study, we also showed different grade of amyloidosis in the atria; the LA was more involved than the RA. This finding corresponds with that of Šteiner et al. (23) and of Leone et al. (14).

Irregular distribution of structural and ultrastructural findings (interstitial fibrosis, distribution of capillaries and cardiomyocyte ultrastuctural changes) in the atrial walls was reported by Corradi et al. (3, 4) who showed most advanced findings in the LA posterior wall in comparison with LA appendage.

Other morphological changes followed in our study were heart weight and LA volume. The hearts of patients with AF were significantly heavier (more hypertrophied) than control hearts. The heaviest hearts were noted in AFF subgroup. Clinical studies, understandably, evaluate rather LA size and its relation to fixation of AF and its progression into the more sustained forms. Kerr et al. (12) who studied a group of 757 patients with paroxysmal AF concluded that LA enlargement is an independent risk factor for AF progression into the "chronic form". Similarly Pillarisetti et al. (19) studying a group of 437 patients demonstrated that in patients with valvular disease and enlarged LA paroxysmal AF has a tendency to get fixed. The relation of LA dilatation to AF was documented in a number of clinical studies by means of ultrasound, magnetic resonance or computed tomography. Also large population studies demonstrate that LA size is closely related to AF progression, e.g. the Framingham study, which prospectively followed up adults after routine surveillance M-mode echocardiograms, showed that left atrial size is an independent risk factor for the subsequent development of AF with a hazard ratio of 1.39 for every 5-mm incremental increase in left atrial size (22). Prospective ultrasound studies showed that AF itself leads to LA dilatation. So, a next vicious circle in etiopathogenesis of AF is completed (4).

Our findings in necropsy patients correlate with the above cited clinical studies. Patients with AF had significantly larger left atria than controls. The largest atria were observed in patients with AF present on their last ECG record before death (AFF).

To assess a possible relation of structural changes of atrial myocardium to conduction characteristics (P wave, QRS complex), we compared the group with most severe amyloidosis (IAA 3) with that with no amyloid detected (IAA 0). There was no difference in either characteristics. This findings is in accordance with that of Ariyarajah et al. (2). On the other hand, Röcken et al. (19), examining RA appendages resected during cardiac surgery in 245 patients, showed that presence of amyloid correlates with P wave length. He deduced that amyloid deposits interfere with atrial conduction properties.

In our comparison of the IAA 3 vs. IAA 0 we have, however, noticed one interesting finding concerning length of the P wave. (Normal P wave length is 110 ms). In the IAA 3 group, frequency of the long P wave ($\geq$ 120 ms) was 35%, while in the IAA 0 it was 25%. Vast majority of these long P wave cases came from hearts with fibrillation subgroup AFS. When comparing the AFS subgroup (composed primarily of cases with newly diagnosed or paroxysmal AF) and the controls with sinus rhythm, we noticed a marked difference in incidence of long P waves: 46% in AFS vs. 14% in controls. Thus, it seems that in patients with AF, who actually present with sinus rhythm, it is more probable that on this ECG there will be an abnormally long P wave than in patients with no history of AF. As we did not find any difference in length of P wave in patients with severe amyloidosis of the atrial myocardium compared to those with no amyloid, we speculate that elongation of P wave is due to dilatation of the LA rather than to the structural change.

Again, the question appears, what is the role of IAA in pathogenesis of AF? Seemingly, amyloid is not a strong predictor of AF and at the same time, AF does not belong to main risk factors for development of amyloid. We must also take into account that IAA is generally much more common than AF – the prevalence of AF in octogenerians is approximately 10%, while that of IAA at this age is almost 90%. The finding that patients with AF have markedly more severe amyloidosis than control patients with sinus rhythm seems to indicate that the effect of AF on the presence of amyloid has a character of modulation rather than of direct formation. There seems no doubt that IAA is a structural change closely related to AF. Fibrillar forms of ANP induce apoptosis and the amyloid deposits impair contractility and conduction properties of cardiomyocytes. Thus, atrial amyloidosis is yet another of vicious circles accompanying AF. Presence of amyloid predicts AF, and, at the same time, AF increases severity of amyloid deposits (21).

Study limitations. We are aware that particularly the clinical part of our study carries several limitations. Firstly, there is a non-uniformity in classifying the arrhythmia in the clinical documentation. Although in most cases the AF is clearly specified, there are other with a rather vague statement of "chronic AF", or even no specification of AF at all.

Certain limitation regards also evaluation of the ECG records. We did not take into consideration individual patient's medication with its possible influence on the ECG parameters. And we had to disregard several ECGs because of artifacts, myocardial infarction, or artificial stimulation.

There is also certain limitation regarding the slightly lower average age of control (sinus) patients compared to those of the study (AF) group. However, when comparing certain parameters between study group and more precisely age-matched but in number significantly reduced control group (35 instead 46 subjects), the results were comparable. This fact is consistent with already cited claim of Platonov et al. (20) that atrial myocardial structural abnormalities are related to presence and duration of AF, and not to the patient age. It seems, that lower average age of control patients led also to higher presence of cardiovascular diseases in AF group compared to control group. We are aware of fact, that higher prevalence of systemic hypertension could affect the severity of structural changes of atrial myocardium in AF group. But still, when using for comparison more precisely age-matched reduced control group, the results were comparable. (There were 14 (30%) patients of control group without history of systemic hypertension, when disregarded patient younger than 68 years old than only 3 (7%) patients remained.)

Conclusion

Our study of necropsy patients showed that patients with a history of atrial fibrillation have, in comparison with those with sinus rhythm, more hypertrophied heart, more voluminous left atrium, more scarring of left atrial myocardium, and more deposits of isolated atrial amyloid. Distribution of atrial myocardial fibrosis and amyloidosis was irregular; the most affected region was left atrial anterior wall.

Correlation of atrial morphology with ECG records revealed an interesting finding – in patients with more severe atrial amyloidosis and history of atrial fibrillation, with sinus rhythm recorded on their last ECG, there is a tendency for prolongation of the P wave, when compared with controls. Thus, finding of long P wave may contribute to diagnosis of a hitherto undisclosed atrial fibrillation.

Acknowledgements

The authors would like to thank Vignendra Ariyrajah, MD and Jiří Nový, MD for ECG evaluation and RNDr. Eva Čermáková for statistical analysis.

The study was supported by grant BBMRI LM2010004, by Charles University Research Development Schemes (PRVOUK) P37/11 and by Specific Academic Research Projects Competition 266902.

References

1. Allessie M, Ausma J, Schotten U. Electrical, contractile and structural remodeling during atrial fibrillation. Cardiovasc Res 2002; 54(2): 230–46.
2. Ariyarajah V, Steiner I, Hájková P et al. The association of atrial tachyarrhythmias with isolated atrial amyloid disease: preliminary observations in autopsied heart specimens. Cardiology 2009; 113: 132–137.
3. Casaclang-Verzosa G, Gersh BJ, Tsang TS. Structural and functional remodeling of the left atrium: clinical and therapeutic implications for atrial fibrillation. J Am Coll Cardiol 2008; 51(1): 1–11.
4. Corradi, D. Atrial fibrillation from the pathologist's perspective. Cardiovasc Pathol 2014; 23(2): 71–84.
5. Corradi D, Callegari S, Benussi S et al. Regional left atrial interstitial remodeling in patients with chronic atrial fibrillation undergoing mitral-valve surgery. Virchows Arch 2004; 445(5): 498–505.
6. Corradi D, Callegari S, Benussi S et al. Myocyte changes and their left atrial distribution in patients with chronic atrial fibrillation related to mitral valve disease. Hum Pathol 2005; 36(10): 1080–9.
7. Čihák R, Heinc P, Haman L, Fiala M, Neužil P, Toman O. Fibrilace síní. Cor Vasa 2011; 53(Suppl 1): 27–52.
8. De Vos CB, Pisters R, Nieuwlaat R et al. Progression from paroxysmal to persistent atrial fibrillation clinical correlates and prognosis. J Am Coll Cardiol 2010; 55(8): 725–31.
9. Eckstein J, Verheule S, de Groot NM, Allessie M, Schotten U. Mechanisms of perpetuation of atrial fibrillation in chronically dilated atria. Prog Biophys Mol Biol 2008; 97(2–3): 435–51.
10. Haïssaguerre M, Jaïs P, Shah DC et al. Spontaneous initiation of atrial fibrillation by ectopic beats originating in the pulmonary veins. N Engl J Med 1998; 339(10): 659–66.
11. Kautzner, J et al. Fibrilace síní v běžné praxi. Praha: Maxdorf Jessenius 2012.
12. Kerr CR, Humphries KH, Talajic M et al. Progression to chronic atrial fibrillation after the initial diagnosis of paroxysmal atrial fibrillation: results from the Canadian Registry of Atrial Fibrillation. Am Heart J 2005; 149(3): 489–96.
13. Kuppahally SS, Akoum N, Burgon NS, et al. Left atrial strain and strain rate in patients with paroxysmal and persistent atrial fibrillation: relationship to left atrial structural remodelling detected by delayed-enhancement MRI. Circ Cardiovasc Imaging 2010; 3: 231–239.
14. Leone O, Boriani G, Chiappini B et al. Amyloid deposition as a cause of atrial remodelling in persistent valvular atrial fibrillation. Eur Heart J 2004; 25(14): 1237–41.
15. Lloyd-Jones DM, Wang TJ, Leip EP et al. Lifetime risk for development of atrial fibrillation: the Framingham Heart Study. Circulation 2004; 110(9): 1042–6.
16. Lukl, Jan. Fibrilace síní. Praha: Grada Publishing, a.s., 2009.
17. Marchese P, Bursi F, Delle Donne G et al. Indexed left atrial volume predicts the recurrence of non-valvular atrial fibrillation after successful cardioversion. Eur J Echocardiogr 2011; 12(3): 214–21.
18. Matějková A, Šteiner I. Morfologické a elektrofyziologické změny srdečních síní zemřelých s fibrilací síní – pilotní studie. Cesk Patol 2014; 50(4): 150–4.
19. Pillarisetti J, Patel A, Boc K et al. Evolution of paroxysmal atrial fibrillation to persistent or permanent atrial fibrillation: predictors of progression. J Atr Fibrillation 2009; 1(7): 388–394.
20. Platonov PG, Mitrofanov LB, Orshanskaya V, Ho SY. Structural abnormalities in atrial walls are associated with presence and persistency of atrial fibrillation but not with age. J Am Col Cardiol 2011; 58: 2225–32.
21. Röcken C, Peters B, Juenemann G et al. Atrial amyloidosis: an arrhythmogenic substrate for persistent atrial fibrillation. Circulation 2002; 106(16): 2091–7.
22. Saffitz JE, Schuessler RB. Altered atrial structure begets atrial fibrillation, but how? J Cardiovasc Electrophysiol 2004; 15(10): 1175–6.
23. Šteiner I, Hájková P. Patterns of isolated atrial amyloid: A study of 100 hearts on autopsy. Cardiovasc Pathol 2006; 15(5): 287–290.
24. Vaziri SM, Larson MG, Benjamin EJ, Levy D. Echocardiographic predictors of nonrheumatic atrial fibrillation. The Framingham Heart Study. Circulation 1994; 89(2): 724–30.

Received: 18/03/2016
Accepted: 30/05/2016

ORIGINAL ARTICLE

Improvement of Anaemia in Patients with Primary Myelofibrosis by Low-Dose Thalidomide and Prednisone

Petra Bělohlávková[1,*], Vladimír Maisnar[1], Jaroslava Voglová[1], Tomáš Buchler[2], Pavel Žák[1]

[1] 4th Department of Internal Medicine - Hematology, Charles University, Faculty Hospital and Faculty of Medicine in Hradec Králové, Hradec Králové, Czech Republic
[2] Department of Oncology, First Faculty of Medicine and Thomayer Hospital, Prague, Czech Republic
* Corresponding author: 4th Department of Internal Medicine – Hematology, University Hospital Hradec Králové, Sokolská 581, 500 05, Czech Republic; e-mail: belohlavkova@fnhk.cz

Summary: Background: A combination of low-dose thalidomide and corticosteroids is a treatment option for anaemic patients with primary myelofibrosis (PMF) who are not eligible for allogeneic hematopoietic stem cell transplantation. Methods: We describe the outcomes of 13 patients with PMF treated with thalidomide 50 mg daily in combination with prednisone 0.5 mg/kg daily. Treatment responses were seen in 10/13 (77%) patients with a median onset of therapeutic effect at 4 weeks (range 3–7 weeks) after treatment initiation. Improvements of anaemia and thrombocytopenia and reduction in splenomegaly were observed in 70%, 38%, and 30% of patients, respectively. Four of six initially transfusion-dependent patients became transfusion independent following the therapy. The median duration of treatment response was 18 months (range 3–35 months). The treatment was well tolerated, with only one patient discontinuing therapy due to toxicity. Responders included both patients with and without JAK2 V617F, and included patients with both newly diagnosed and longstanding PMF. Conclusions: Our retrospective analysis confirmed that the therapy with low-doses thalidomide with prednisone in patients with PMF achieves significant response rate in anaemia with low treatment toxicity.

Keywords: *Primary myelofibrosis; Immunomodulatory agents; Thalidomide; Treatment*

Introduction

Primary myelofibrosis (PMF) is a clonal disorder of haematopoiesis from the group of Philadelphia-negative myeloproliferative diseases. The median survival of patients with PMF is approximately 3.5 to 10 years depending on the presence of risk factors such as higher age, anaemia, blasts in peripheral blood, and constitutional symptoms. The International Prognostic Scoring System (IPSS) and the Dynamic IPSS (DIPSS) are used to stratify patients into risk groups and to select appropriate treatment (1–4).

Younger patients (<65–70 years) with advanced disease should be considered for allogeneic haematopoietic stem cell transplantation (HSCT). HSCT remains the only curative treatment option for PMF (5–11). In contrast, conventional treatments are intended to influence the main symptoms of PMF resulting from splenomegaly and anaemia and to maintain or improve the quality of life but have no or minimal impact on the survival of patients. Anaemia is often the most disabling symptom of PMF, being present in about 20% of patients at diagnosis and in up to 50% of patients after 3.5 years of disease duration. Various drugs including danazol and erythropoietin have been proposed for the treatment of anaemia in the past but are usually ineffective for PMF-associated anaemia (12, 13).

Immunomodulatory drugs (IMiDs) such as thalidomide, lenalidomide, and pomalidomide have recently been shown to improve anaemia associated with PMF. These agents exhibit pleiotropic effects, reducing the levels of cytokines (transforming growth factor-beta, platelet-derived growth factor), inhibiting angiogenesis (vascular endothelial growth factor, basic fibroblastic growth factor), and triggering immunomodulation (increased production of T cells and NK cells). Other mechanisms of action that may be beneficial in patients with PMF include the induction of apoptosis by inhibition of nuclear kappa B (NF κ-B) and by activation of the caspase-8 death receptor pathway (14). Thalidomide and pomalidomide have also been found to be potent regulators of erythropoiesis, promoting the survival of erythrocyte progenitors and increasing the expression of foetal haemoglobin (HbF) (15).

Several groups have published reports on treatment of PMF using thalidomide at different doses ranging from 50 to 800 mg per day. Improvements of anaemia in these studies have been achieved in 16 to 70% of patients. However, up to 50% of patients receiving higher doses of thalidomide had to discontinue the treatment due to adverse events. In an effort to reduce the toxicity, we have explored a treatment regimen using low-dose thalidomide (50 mg daily) in combination with prednisone (0.5 mg/kg/day). The treat-

http://dx.doi.org/10.14712/18059694.2016.89

ment produced significant clinical benefit with markedly low toxicity (16–22).

Patients and Methods

Thirteen patients (10 men, 3 women) were treated with low-dose thalidomide with prednisone in the period from 11/2005 to 7/2015 at our institution. All patients had a primary form of PMF. The median age was 66 years (range 52–81 years) and 5/13 (38%) patients were positive for JAK2V617 mutation. The median time from diagnosis to the start of thalidomide treatment was 22 months (range 1–156 months).

Symptoms resulting from progressive anaemia were the reason for treatment initiation in all patients. Six patients were transfusion-dependent prior to the onset of therapy. In all cases, patients received no previous therapy for PMF. Initial median values at the start of treatment were as follows: haemoglobin 8 g/dL (range 6–9 g/dL), platelet count 182 × 10^9/L (range 15–650 × 10^9/L), leukocyte count 5.93 × 10^9/L (range 2.64 – 13.6 × 10^9/L), and the median initial palpable spleen size was 10 cm below the costal margin (range 1–15 cm).

Treatment with thalidomide 50 mg daily and prednisone 0.5 mg/kg/day was administered for at least 3 months and was then discontinued if no therapeutic effect was seen. After 3 months of treatment, the dose of prednisone was gradually tapered to a maintenance dose of 5 to 10 mg/day in patients with ongoing treatment.

Therapeutic responses were evaluated according to the International Working Group – Myeloproliferative Neoplasms Research and Treatment (IWG-MRT) and European Leukemia Net (ELN) criteria (23).

Results

Therapeutic responses were achieved in 10/13 (77%) patients. According to the IWG-MRT criteria, five patients achieved partial remission (PR) and further five patients clinical improvement (CI). Peripheral blood parameters of patients after 3 months of treatment were as follows: median haemoglobin 9.9 g/dL (range 8–10.6 g/dL), median platelet count 251 × 10^9/L (range 87–1020 × 10^9/L), median leukocyte count 6.31 × 10^9/L (range 4.01–18.67 × 10^9/L). In 5/13 (38%) patients, there was an increase in platelet count ≥ 50% of the initial values and 4/13 patients (30%) had a reduction in spleen size of ≥ 50% compared to the initial size. Transfusion dependence resolved in 4/6 initially transfusion-dependent patients.

In accordance with published data, the treatment responses occurred rapidly, after median treatment duration of only four weeks (range 3–7 weeks). The median duration of response was 15 months (range 3–35 months). Responders included both patients with and without JAK2 V617F, and included patients with both newly diagnosed and long-standing PMF.

Summary of patient characteristics and treatment responses is shown in Table 1.

Tab. 1: Characteristics for 13 patients with PMF treated by low-dose thalidomide with prednisone.

Sex	Age	DIPSS	JAK2 status	Time from diagnosis (months)	Transfusions requirement	Time to response (weeks)	IWG-MRT response	Response duration (months)	Adverse events	Reasons of withdrawal therapy
F	52	High	neg	156	no	5	PR	35	–	HSCT
F	76	High	pos	22	yes	4	PR	34	neuropathy	death (CV reason)
M	66	High	neg	3	yes	6	CI	25	–	lack of effect
M	55	High	neg	30	yes	4	CI	3	neutropenia gr. II, pneumonia	adverse events
F	57	High	neg	146	no	3	CI	5	constipation	HSCT
M	69	High	neg	9	yes	–	SD	–	–	
M	64	Int-2	neg	54	no	–	SD	–	–	
M	79	High	neg	1	no	5	CI	14	–	lack of effect
M	72	High	pos	1	no	3	PR	10	–	lack of effect
M	81	High	pos	3	yes	3	PR	12	neuropathy, tiredness	continuing
M	68	High	pos	6	yes	–	SD	–	–	
M	57	Int-1	pos	108	no	6	PR	20	tiredness	continuing
M	59	Int-1	neg	39	no	3	CI	20	–	continuing

Haematological toxicity led to treatment discontinuation in a single patient who developed grade 2 neutropenia with infection, and even in that patient anaemia had improved. No thrombotic complications were seen. Antithrombotic prevention was not routinely applied but was administered in one elderly patient with cardiovascular risk factors. Non-haematological toxicity was observed in four patients, including two cases of grade 1–2 neuropathy with worsening of chronic constipation in one of the two patients, and fatigue in two other patients. The reason for treatment discontinuation was allogeneic unrelated transplantation in two patients. In three cases, treatment was discontinued after 9, 14, and 25 months, respectively, because of the loss of therapeutic effect. One patient died of a cardiovascular cause unrelated to PMF (end stage of heart failure).

Discussion

Several series and case studies have been published on the possible use of IMiDs therapy in patients with PMF. The first experience was published in 2001 by Barosi et al. (16), reporting on a group of 21 patients treated with an initial thalidomide dose of 100 mg daily and gradually increased to 400 mg daily. Therapeutic responses were achieved in 13 patients (62%), including improvement of anaemia, thrombocytopenia, and reduction of spleen size in 43%, 67%, and 31% of patients, respectively. However, 91% of patients discontinued the treatment within 6 months due to toxicity or lack of treatment response.

Elliott et al. (17) used thalidomide in a dose of 200–400 mg daily in a series of 15 patients with similar results, achieving improvements of anaemia and thrombocytopenia, and reduction in spleen size in 20%, 60%, and 25% of patients, respectively. Again, premature treatment discontinuation was required in 80% of patients.

In the largest study (n = 63) to-date which was published in 2004 by Marchetti et al. (18), the doses of thalidomide ranged from 50 to 400 mg daily. In 11 patients (26%), the treatment had beneficial effect on anaemia, including eight patients who became transfusion independent. Improvements in thrombocytopenia occurred in 22% of patients and a reduction in spleen size in 19% of patients. The median tolerated dose of thalidomide in this study was 100 mg daily, and only 13% of patients tolerated a higher dose. Despite this relatively low dose of thalidomide, a high proportion of patients (49%) discontinued the therapy due to toxicity during the first six months after its initiation.

The cohort published by Thomas et al. (19) included 44 patients who received thalidomide in a dose of 100–800 mg daily. Treatment responses were achieved in 41% of patients, with 20% patients experiencing improvement of anaemia and 21% of thrombocytopenia, and

31% a reduction in spleen size. These studies have shown that although intermediate and high doses of thalidomide may accomplish some clinical objectives, they are generally poorly tolerated. In these studies, haematological toxicity prompted treatment discontinuation in 25–91% of patients. The obvious way forward was to explore the effect of low-dose thalidomide and look for possible combination regimens.

In 2003, Mesa et al. (20) published a paper describing the effect of thalidomide 50 mg daily and 30 mg of prednisone given daily over three months in a group of 21 patients. An increase in haemoglobin was observed in 70% of patients and 40% of patients became transfusion independent. Improvements in platelet counts occurred in 75% of patients but only 19% of patients had a reduction in spleen size. The response usually persisted even after gradual discontinuation of corticosteroids. In this study, only 5% of patients discontinued treatment due to adverse events.

Similar results were obtained in a 2008 study by Weinkove et al. (21), in which 15 patients were treated with thalidomide 50 mg daily and 13 of them also received concomitant prednisone 30–60 mg daily. The responses evaluated according to the European Network for Myelofibrosis (EUMNET) criteria (24) were as follows: 27% of patients achieved a major response, 7% a moderate response, and 33% a minor response, while 27% had no treatment response. Only three patients discontinued treatment because of toxicity. The median time to best response was 7.5 weeks (range 2–15 weeks).

Another recent work using a combination of thalidomide with corticosteroids was published in 2011 by Thapaliya et al. (25). Their cohort included 50 patients with PMF divided into three arms. All patients received 50 mg of thalidomide with low-dose corticosteroids. The first subgroup received no additional treatment, cyclophosphamide 25 mg daily was added to the second group, and etanercept 25 mg twice weekly was added in the third subgroup. Therapeutic responses were achieved in 28% of patients and the response rates were similar in all three study arms, suggesting no benefit of cyclophosphamide or etanercept. Improvement of anaemia was the most commonly observed type of response, occurring in 22% of patients, while 8% of patients had a reduction in spleen size. The median duration of response reached 8.5 months. A possible synergistic action of corticosteroids may potentiate the cytotoxic effect of IMiDs, reducing the levels of some interleukins and possibly decreasing the toxicity of IMiDs treatment.

Several studies have been published on the treatment of PMF with IMiDs other than thalidomide (lenalidomide, pomalidomide) (26–29). In studies, lenalidomide has been associated with the lower response rates and higher toxicity (myelosuppression). The response rates achieved with pomalidomide are similar to those of thalidomide, ranging from 19 to 30%. The principal disadvantage of pomalidomide is the high cost of treatment and the risk of myelosuppression which can occur in as many as 25–88% of patients. In 2010, the first results were published of a multicentre study using pomalidomide 2 mg/day plus placebo, pomalidomide 2 mg/day plus prednisone, pomalidomide

0.5 mg/day plus prednisone and prednisone plus placebo (29). Response rates for clinical improvement in anaemia were 23%, 16%, 36% and 19% in the four arms. The results of this trial demonstrated once again that the best effect in PMF can be expected with the combination of low-dose IMiDs with prednisone.

Conclusion

Our retrospective analysis confirmed that therapy with low-doses thalidomide with prednisone in patients with PMF achieves significant response rate in anaemia with low treatment toxicity. A clinically meaningful increase in haemoglobin levels was observed in 10/13 (77%) patients. The onset of response was very rapid and the median duration of response was 15 months. Responders included both patients with and without JAK2 V617F. The use of low-dose IMiDs in combination with corticosteroids thus represents a valid therapeutic option for patients with PMF who are not eligible for allogeneic HSCT.

References

1. Tefferi A. Myelofibrosis with myeloid metaplasia. N Engl J Med 2000; 342: 1255–1265.
2. Dupriez B, Morel P, Demory JL, et al. Prognostic factors in agnogenic myeloid metaplasia: a report on 195 cases with a new scoring system. Blood 1996; 88: 1013–1018.
3. Cervantes F, Dupriez B, Pereira A, et al. New prognostic scoring system for primary myelofibrosis based on a study of the International Working Group for Myelofibrosis Research and Treatment. Blood 2009; 113(13): 2895–2901.
4. Passamonti F, Cervantes F, Vannucchi AM, et al. A dynamic prognostic model to predict survival in primary myelofibrosis: A study by the IWG-MRT (International Working Group for Myeloproliferative Neoplasms Research and Treatment). Blood 2010; 115: 1703–1708.
5. Rondelli D, Barosi G, Bacigalupo A, et al. Myeloproliferative Diseases Research Consortium. Allogeneic hematopoietic stem-cell transplantation with reduced-intensity conditioning in intermediate- or high-risk patients with myelofibrosis with myeloid metaplasia. Blood 2005; 105: 4115–9.
6. Kroeger N, Holler E, Kobbe G, et al. Dose-reduced conditioning followed by allogeneic stem cell transplantation in patients with myelofibrosis. Results from a multicenter prospective trial of the Chronic Leukemia Working Party of the European Group for Blood and Marrow Transplantation (EBMT). Blood 2007; 110: 210a.
7. Zang DY, Deeg HJ. Allogeneic hematopoietic cell transplantation for patients with myelofibrosis. Curr Opin Hematol 2009; 16(2): 140–146.
8. Ballen KK, Shrestha S, Sobocinski KA, et al. Outcome of transplantation for myelofibrosis. Biol Blood Marrow Transplant 2010; 16: 358–367.
9. Abelsson J, Merup M, Birgegard G, et al. The outcome of allo-HSCT for 92 patients with myelofibrosis in the Nordic countries. Bone Marrow Transplant 2012; 47(3): 380–386.
10. Babushok D, Hexner E. Allogeneic transplantation for myelofibrosis: for whom, when,and what are the true benefits? Curr Opin Hematol 2014; 21(2): 114–122.
11. Gupta V, Malone AK, Hari PN. Reduced-intensity hematopoietic cell transplantation for patients with primary myelofibrosis: a cohort analysis from the center for international blood and marrow transplant research. Biol Blood Marrow Transplant 2014; 20(1): 89–97.
12. Cervantes F, Alvarez-Larran A, Domingo A, Arellano-Rodrigo E, Montserrat E. Efficacy and tolerability of danazol as a treatment for the anaemia of myelofibrosis with myeloid metaplasia: long-term results in 30 patients. Br J Haematol 2005; 129(6): 771–775.
13. Huang J, Tefferi A. Erythropoiesis stimulating agents have limited therapeutic activity in transfusion-dependent patients with primary myelofibrosis regardless of serum erythropoietin level. Eur J Haematol 2009; 83(2): 154–155.
14. Tabarroki A, Tiu R. Immunomodulatory agents in myelofibrosis. Expert Opin Investig Drugs 2012; 21(8): 1141–54.
15. Moutouh-de Parseval LA, Verhelle D, Glezer E, et al. Pomalidomide and lenalidomide regulate erythropoiesis and fetal hemoglobin production in human CD34+ cells. J Clin Invest 2008; 118(1): 248–258.
16. Barosi G, Grossi A, Comotti B, Musto P, Gamba G, Marchetti M. Safety and efficacy of thalidomide in patients with myelofibrosis with myeloid metaplasia. Br J Haematol 2001; 114(1): 78–83.
17. Elliott MA, Mesa RA, Li CY, et al. Thalidomide treatment in myelofibrosis with myeloid metaplasia. Br J Haematol 2002; 117(2): 288–96.
18. Marchetti M, Barosi G, Balestri F, et al. Low-dose thalidomide ameliorates cytopenias and splenomegaly in myelofibrosis with myeloid metaplasia: a phase II trial. J Clin Oncol 2004; 22(3): 424–31.
19. Thomas DA, Giles FJ, Albitar M, Cortes JE, et al. Thalidomide therapy for myelofibrosis with myeloid metaplasia. Cancer 2006; 106(9): 1974–84.
20. Mesa RA, Steensma DP, Pardanani A, et al. A Phase 2 trial of combination low-dose thalidomide and prednisone for the treatment myelofibrosis with myeloid metaplasia. Blood 2003; 101: 2534–2541.
21. Weinkove R, Reilly JT, McMullin MF, Curtin NJ, Radia D, Harrison CN. Low-dose thalidomide in myelofibrosis. Haematologica 2008; 93(7): 1100–1.
22. Holle N, de Witte T, Mandigers C, Schaap N, Raymakers R. Thalidomide and lenalidomide in primary myelofibrosis. Neth. J Med 2010; 68(1): 293–8.
23. Tefferi A, Cervantes F, Mesa R, et al. Revised response criteria for myelofibrosis: International Working Group-Myeloproliferative Neoplasms Research and Treatment (IWG-MRT) and European LeukemiaNet (ELN) consensus report. Blood 2013: 22; 122(8): 1395–8.
24. Barosi G, Bordessoule D, Briere D, et al. Response criteria for myelofibrosis with myeloid metaplasia: results of an initiative of the European Myelofibrosis Network (EUMNET). Blood 2005; 106(8): 2849–2853.
25. Thapaliya P, Tefferi A, Pardanani A, et al. International working group for myelofibrosis research and treatment response assessment and long-term follow-up of 50 myelofibrosis patients treated with thalidomide-prednisone based regimens. Am J Hematol 2011; 86(1): 96–98.
26. Tefferi A, Cortes J, Verstovsek S, et al. Lenalidomide therapy in myelofibrosis with myeloid metaplasia. Blood 2006; 108(4): 1158–64.
27. Quintas-Cardama A, Kantarjian HM, Manshouri T, et al. Lenalidomide plus prednisone results in durable clinica; histopahtologic, and molecular responses in patients with myelofibrosis. J Clin Oncol 2009; 27(28): 4760–6.
28. Mesa RA, Yao X, Cripe LD, et al. Lenalidomide and prednisone for myelofibrosis: Eastern Cooperative Oncology Group (ECOG) phase 2 trial E4903. Blood 2010; 25; 116(22): 4436–8.
29. Mesa RA, Pardanani AD, Hussein K, et al. Phase1/-2 study of Pomalidomide in myelofibrosis. Am J Hematol 2010; 85(2): 129–30.

Received: 02/03/2016
Accepted: 21/03/2016

ORIGINAL ARTICLE

Carrier Molecules and Extraction of Circulating Tumor DNA for Next Generation Sequencing in Colorectal Cancer

Martin Beránek[1,2,], Igor Sirák[3], Milan Vošmik[3], Jiří Petera[3], Monika Drastíková[1], Vladimír Palička[1]*

[1] Institute of Clinical Biochemistry and Diagnostics, University Hospital Hradec Králové, Charles University, Faculty of Medicine in Hradec Králové, Czech Republic
[2] Department of Biochemical Sciences, Charles University, Faculty of Pharmacy in Hradec Králové, Czech Republic
[3] Department of Oncology, University Hospital Hradec Králové, Charles University, Faculty of Medicine in Hradec Králové, Czech Republic
* Corresponding author: Institute of Clinical Biochemistry and Diagnostics, University Hospital Hradec Králové, Sokolská 581, 500 05 Hradec Králové, Czech Republic; e-mail: beranek@lfhk.cuni.cz

Summary: The aims of the study were: *i*) to compare circulating tumor DNA (ctDNA) yields obtained by different manual extraction procedures, *ii*) to evaluate the addition of various carrier molecules into the plasma to improve ctDNA extraction recovery, and *iii*) to use next generation sequencing (NGS) technology to analyze *KRAS*, *BRAF*, and *NRAS* somatic mutations in ctDNA from patients with metastatic colorectal cancer. Venous blood was obtained from patients who suffered from metastatic colorectal carcinoma. For plasma ctDNA extraction, the following carriers were tested: carrier RNA, polyadenylic acid, glycogen, linear acrylamide, yeast tRNA, salmon sperm DNA, and herring sperm DNA. Each extract was characterized by quantitative real-time PCR and next generation sequencing. The addition of polyadenylic acid had a significant positive effect on the amount of ctDNA eluted. The sequencing data revealed five cases of ctDNA mutated in *KRAS* and one patient with a *BRAF* mutation. An agreement of 86% was found between tumor tissues and ctDNA. Testing somatic mutations in ctDNA seems to be a promising tool to monitor dynamically changing genotypes of tumor cells circulating in the body. The optimized process of ctDNA extraction should help to obtain more reliable sequencing data in patients with metastatic colorectal cancer.

Keywords: *Carrier; Extraction; Circulating tumor DNA; Next generation sequencing; Real-time PCR*

Introduction

In mammalian cells, deoxyribonucleic acid saving genetic information is located in nucleus and mitochondria. Low amounts of genomic DNA are released into the blood plasma as cell-free DNA (cfDNA) with a median half-life of 16 minutes (1). In healthy subjects, the cfDNA concentration usually ranges between 0 ng/mL and 100 ng/mL. This corresponds to 0–15,150 genome equivalents per mL (GE/mL) (2). Numerous studies reported elevated cfDNA in pregnancy (fetal DNA), inflammation, autoimmune diseases, acute rejection of transplants, sepsis, or cancer (3–6), where circulating tumor-derived DNA (ctDNA) could reach hundreds of ng/mL (2, 7). In metastatic patients with increased ctDNA, the overall two-year survival rate of 48% was described (8).

Cell-free DNA is formed by 100–200 bp chromosomal fragments with the appropriate length of 311 nm (9). These short fragments were found in the plasma of both patients with malignancies or benign polyps, and/or healthy individuals (10, 11). Integral DNA molecules in plasma, on the other hand, originate from leukocytes or viable circulating tumor cells (12).

Previously published papers showed that somatic mutations in the *KRAS* (Kirsten rat sarcoma viral oncogene homolog) gene are often present in ctDNA of individuals suffering from pancreatic or gastrointestinal tumors (13). The mutations in *KRAS* codons 12, 13, and 61 were observed in plasma of one-fourth of metastatic cases, and an 80–86% mutation match between primary tumor tissues and ctDNA was demonstrated (14, 15).

Since the determination of the mutation status in the tumor tissue is necessary for the indication of targeted biological treatment of metastatic colorectal cancer, a panel of mutations tested in *KRAS* and other genes is being completed. In their analysis, sensitive investigation methods including real-time PCR, digital PCR, COLD PCR, reverse hybridization strips, or next generation sequencing have been applied. In this context, a clinical benefit of ctDNA testing is considered, as well. A reliable analytical process, however, requires relatively high volumes of plasma and the highest ctDNA concentrations in extracts possible.

The aims of the study were: *i*) to compare ctDNA yields obtained by four different manual extraction procedures, *ii*) to evaluate the addition of various carrier molecules

ACTA MEDICA (Hradec Králové) 2016; 59(2):54–58
http://dx.doi.org/10.14712/18059694.2016.54

into the plasma to improve ctDNA extraction recovery, and *iii*) to use next generation sequencing (NGS) technology to analyze *KRAS*, *BRAF* (B-raf proto-oncogene), and *NRAS* (neuroblastoma rat sarcoma viral oncogene homolog) somatic mutations in ctDNA from patients with metastatic colorectal cancer.

Material and Methods

Subjects

Venous blood with EDTA (9–10 mL) was obtained from thirty-two patients of the Department of Oncology, University Hospital in Hradec Králové who suffered from metastatic colorectal carcinoma. The experimental group consisted of 17 men and 15 women with a median age of 72 years (range 60–83 years). The diagnosis of metastatic disease was based on computer tomography examination. The standard clinical and histopathological classification of tumors was performed, including molecular analysis of *KRAS*, *BRAF*, and *NRAS* in formalin-fixed paraffin-embedded (FFPE) tumor tissue specimens. Histological verification of metastatic lesions was not required. The collections were performed with their informed consent.

Extraction of ctDNA

Within 1 h after collection, the blood specimens were centrifuged at 1300 g at 25 °C for 10 min; 2–3 mL supernatant (part I) was used for the preparation of pooled plasma. Consequently, 800 µL pooled plasma aliquots were spun at 12,000 g at 4 °C for 10 min. The 750 µL supernatant was transferred into a new plastic tube and stored at −20 °C. For ctDNA extraction, the following methods were used according to the manufacturer's instructions adapted to a 750 µL plasma volume: QIAamp DNA Mini Kit (the spin protocol for DNA purification from blood or body fluids; Qiagen, Germany), QIAamp DSP Virus Spin Kit (Qiagen, Germany), NucleoSpin Plasma XS Kit (Macherey-Nagel, Germany), and Agencourt Genfind v2 Kit (Beckman Coulter, USA). The elution volume of TRIS-EDTA buffer was 35 µL. All extractions were performed in hexaplicates.

To evaluate the effectiveness of the used extraction procedures for short (<200 bp) and longer (200–500 bp) ctDNA fragments, 10 µL of GeneScan 500 LIZ Dye Size Standard (Applied Biosystems, UK) was added into another tube with the aliquot, and co-extracted along with ctDNA molecules. Then, fragmentation analysis in the ABI 3130 Genetic Analyzer (Life Technologies, USA) followed. The recovery of fragments was determined by their normalization to the longest (500 bp) fragment and expressed in percentages.

In second part of the study, the following amounts of carriers were added into the 750 µL pooled plasma aliquots: *i*) 17 µg carrier RNA (Qiagen, Germany), *ii*) 4 µg polyadenylic acid (poly(A); Roche Diagnostics, Germany), *iii*) 100 µg ultrapure glycogen (Invitrogen, USA), *iv*) 40 µg linear acrylamide (Invitrogen, USA), *v*) 40 ng yeast tRNA (Invitrogen, USA), *vi*) 40 ng ultrapure salmon sperm DNA (Invitrogen, USA), and *vii*) 40 ng herring sperm DNA (Promega, USA). After that, the extraction process with the NucleoSpin Plasma XS kit was performed as above. The extractions were carried out in hexaplicates, as well.

The third part of the study was focused on individual plasma specimens of the patients. From their residual 1–2 mL plasma (part II), a 750 µL supernatant was obtained as described above. After the addition of 4 µg polyadenylic acid, the extraction of ctDNA was carried out *via* the NucleoSpin Plasma XS kit. The extracts were stored at −80 °C until analysis.

Analysis of ctDNA extracts

Each extract was characterized by quantitative real-time PCR (Rotor-Gene 6000, Corbett Research, Australia) of the *POLR2A* housekeeping gene (gb Genetic Human DNA kit, Generi Biotech, Czech Republic). Using serial dilutions of Generi Biotech Standard Human Positive Control (20 ng/µL), a calibration curve ranging from 1 to 10,000 ng/mL was constructed, and ctDNA amounts in the extracts were determined.

For deep targeted NGS analysis, we used the Somatic 1 Master Kit (Multiplicom, Belgium) which enables molecular diagnostics based on multiplex *BRAF*, *KRAS*, and *NRAS* full exon amplifications (in total 30 amplicons with lengths of 168–255 bp) carried out in the MiSeq sequencing system (MiSeq Reagent Kit v2, 2x250 output; Illumina, USA). Analysis with amplicon-specific tagged primers was performed according to the manufacturer's instructions with 7 µL of ctDNA extracts. As the wild-type control, 7 µL of cfDNA of two healthy subjects were included into each NGS run.

The presence of the mutations in ctDNA was validated by reverse hybridization strip assays: KRAS 12/13/61 StripAssay, BRAF StripAssay, and NRAS XL StripAssay (ViennaLab, Austria). The findings were finally compared with results of the FFPE tumor tissue analysis of the patients performed with the same technology in the frame of the routine diagnostic process. The established sensitivity of the strip technology for the variants was 1%.

Bioinformatical analysis

The secondary sequencing data analysis was initiated by generating raw binary base call files (BCL) from gray scale images of each cluster. For demultiplexing the samples, Illumina *Miseq Reporter* with a set up mismatch of 0 for each barcode was used. Paired FASTQ files were aligned to the reference Human genome HG19 by Burrows-Wheeler Algorithm (BWA) with the binary alignment map (BAM) output format. Variants were detected by Illumina *Somatic Variant Caller Algorithm* performed as a part of secondary analysis performed by *MiSeq Reporter* (MSR). The final variant calling format (VCF) files were annotated using an Illumina

Tab. 1: Concentrations of ctDNA and recoveries of fragments differing in size.

Extraction	DNA concentration Mean (SD) ng/mL	Recovery of fragments*				
		75/500 bp %	100/500 bp %	200/500 bp %	300/500 bp %	400/500 bp %
QIAamp Mini	163 (24)	32	59	89	99	99
Nucleospin	448 (48)**	77	87	95	99	100
DSP Virus	539 (154)**	45	77	98	99	100
Agencourt	223 (69)	0	0	0	32	93

* 500 bp fragments were used as referent; SD standard deviation; ** $P < 0.001$

Variant Studio online tool and visualized in the *Integrative Genomics Viewer* (IGV, Broad Institute of Massachusetts Institute of Technology and Harvard, USA). The detection threshold for mutations was set at 1%. The minimal read depth for detecting pathogenic variants was 100 bases at the given position.

Statistical analysis

Concentrations of ctDNA were evaluated by using the Student t test. The normality of values was evaluated by the Shapiro-Wilk W test. Differences were considered to be statistically significant when $P < 0.05$.

Results

The concentrations of ctDNA in pooled plasma extracts are demonstrated in Table 1. The highest levels of ctDNA were obtained by using the QIAamp DSP Virus Spin (the mean value 539 ng/mL) and NucleoSpin Plasma XS (448 ng/mL) kits. In these extracts, the ctDNA amounts were more than twofold higher than those from the QIAamp Mini Kit (163 ng/mL, $P < 0.001$).

The procedures used differed in terms of the spectrum of DNA fragments extracted. The NucleoSpin method provided the highest extraction efficiency for fragments <200 bp, in which most ctDNA molecules are contained. The Agencourt kit revealed a satisfactory recovery only for DNA fragments longer than 400 bp. Electroferograms for the NucleoSpin Plasma XS and QIAamp DSP Virus Spin fragments are demonstrated in Figure 1.

Figure 2 illustrates the influence of the carrier molecules added into plasma before the Nucleospin extraction procedure. Only the addition of 4 µg polyadenylic acid had a significant positive effect on the amount of ctDNA eluted ($P < 0.05$). The other carriers had none (carrier RNA), or even a negative effect (glycogen, linear acrylamide, yeast tRNA, salmon or herring sperm DNA) on the ctDNA yield. The Nucleospin technology, efficiency of which was enhanced by polyadenylic acid, was further used for individual ctDNA extractions from the thirty-two plasma specimens of the patients. In the extracts, the levels of ctDNA ranged from 50 to 580 ng/mL with a median value of 260 ng/mL.

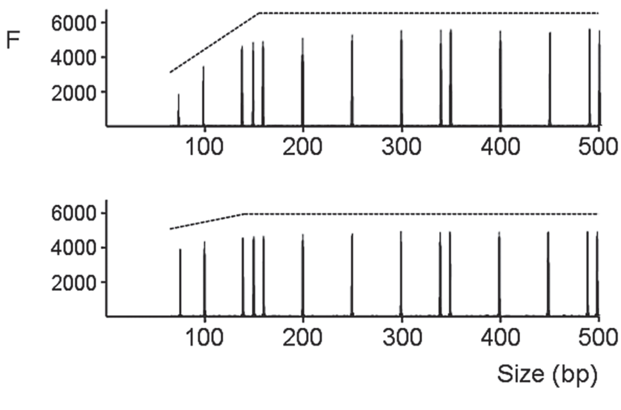

Fig. 1: Extraction recoveries of DNA fragments of GeneScan 500 LIZ Dye Size Standard when added into human plasma and extracted with the QIAamp DSP Virus Spin Kit (upper part) and the NucleoSpin Plasma XS Kit (lower part). Lengths of fragments: 75, 100, 139, 150, 160, 200, 250, 300, 340, 350, 400, 450, 490 and 500 bp. F is fluorescence. The latter extraction procedure showed lower losses of the fragments in the range of 75–200 bp.

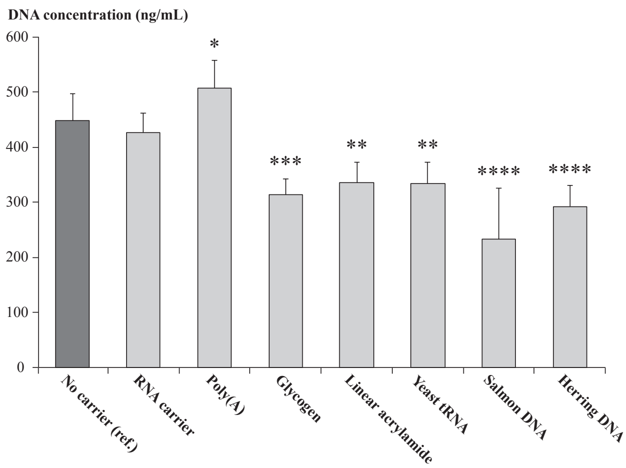

Fig. 2: Concentrations of ctDNA in the NucleoSpin extracts in relation to the used carrier molecule. DNA concentrations are expressed as means and standard deviations; * $P < 0.05$, ** $P < 0.01$, *** $P < 0.002$, **** $P < 0.001$.

The following NGS analysis was successful in all cases; 100% bases in the exons were sequenced bi-directionally. We achieved NGS run metrics as follows: cluster density 678 K/mm^2; total number of reads 14.1 millions; pass filter reads 13.2 millions; mean number of reads 0.5 million per sample; average amplicon coverage 15,000-fold; and the total amount of basecalls >Q30 was 86.0%.

The sequencing data revealed five cases (16%) of ctDNA mutated in *KRAS*. Three patients were mutated in *KRAS* codon 13 (the mutation c.38G>A, p.Gly13Asp, rs112445441 in all three specimens), one in *KRAS* codon 12 (c.35G>T, p.Gly12Val, rs121913529), and another one in *KRAS* codon 61 (c.182A>G, p.Gln61Arg, rs121913240). In *BRAF*, one subject (3%) was found to have p.Val600Glu activating mutation (c.1799T>A, rs113488022). No mutations in the *NRAS* gene were obvious. The results of the ctDNA NGS analysis agreed with those obtained by the reverse hybridization technique, and with the data on FFPE, except one subject with tumor tissue mutated in *KRAS* codon 12 (c.34G>A, p.Gly12Ser, rs121913530) and negative in the corresponding ctDNA specimen. Thus, an agreement of 86% was found between tumor tissues and ctDNA.

Discussion

Knowledge of genetic background helps in selecting an individual approach to metastatic colorectal cancer treatment, including targeted biological therapy. However, primary tumor tissue is not always available, and could be of insufficient quality, or could have been obtained a long time before the metastases were diagnosed. Moreover, several reports have indicated the status of somatic mutations in metastases changes in the course of therapy as a result of tumor heterogeneity, clonal expansion, and selection (16, 17). These changes are responsible for acquired resistance developing within a few months (18). Since invasive and painful biopsies of metastatic tissue are often difficult to obtain, ctDNA testing, available at any disease stage, seems to be a good alternative for analyzing mutations during the follow-up period.

One aim of this study was to increase the efficiency of the ctDNA extraction process, when using 2–3 mL of blood or 750 μL of plasma, respectively, is used. Larger blood collections during the follow-up period of metastatic patients are sometimes difficult to obtain. There are a lot of manufacturers providing commercial products for cfDNA extraction and purification. We examined two of them based on the manual spin technology with (QIAamp DSP Virus Spin Kit) or without the addition of carrier molecules (NucleoSpin Plasma XS Kit), and with a protocol that uses paramagnetic separation beads (Agencourt Genfind v2 Kit). The results were compared to the QIAamp DNA Mini Kit, a universal and robust extraction product used in clinical labs for over fifteen years. For the evaluation, quantitative real-time PCR analysis was preferred to the spectrophotometric and fluorometric measurements that often result in interference of carrier polynucleotide chains and overestimation of low-copy DNA molecules.

Mouliere et al. reported that more than 80% of ctDNA fragments in the plasma of metastatic patients were shorter than 145 bp, with a large proportion of the ctDNA fragments <100 bp (19, 20). Our results revealed that the NucleoSpin Plasma XS process is highly effective for ctDNA fragments in the size range of 75–200 bp, despite the fact that no carrier molecules are used in it. The mean concentration of extracted ctDNA was 448 ng/mL. It corresponded to almost 68,000 GE/mL and agreed with previous studies (7, 19–21).

Next, we studied how the addition of various carrier molecules effects the extraction efficiency. The QIAamp DNA Mini Kit instructions recommend using carrier DNA for extractions of low copy number DNA (<10 000 GE/mL), although the carrier DNA is not included in the kit. In other Qiagen products, carrier RNA molecules are included and used regardless of the ctDNA amounts expected in the specimen. Shaw et al. previously showed that for maximum improvement of the DNA yield, the ideal ratio of carrier RNA to DNA was between 10:1 and 50:1; ratios outside this range do not enhance DNA recovery as successfully (22). We added 4 μg of polyadenylic acid into 750 μL of plasma (ratio 12:1) before the NucleoSpin extraction process, thus increasing the ctDNA yield in eluates.

The addition of poly(A) carrier RNA but not glycogen previously increased the recovery of automated silica-based extractions (BioRobots EZ1 and BioRobots M48, Qiagen) by an average of 24% (23). In another paper, a five-fold increased recovery was obtained in DNA extractions carried out on silica-based monoliths within a microfluidic device when poly(A) carrier RNA was added to the chaotropic salt solution (22). However, the Qiagen carrier RNA added into the plasma specimens of our patients in a ratio of 50:1 (RNA:ctDNA) had no effect on the NucleoSpin ctDNA recovery. Not only the proper carrier RNA:ctDNA ratio but also the length of poly(A) chains and their folding in space probably play an important role in the extraction process.

The remaining carriers reduced the final ctDNA amounts. Cheung et al. reported that the addition of yeast tRNA or salmon sperm DNA prior to purification by silica particles resulted in significantly decreased recovery of HCV RNA from sera (24). Thus, glycogen, linear acrylamide, yeast tRNA, salmon sperm DNA, or herring sperm DNA, are not suitable substances to improve yields of commercial silica-based extraction procedures. On the other hand, when used as co-precipitants, they can facilitate recovery of the target DNA molecules in the phenol/chloroform extraction from eukaryotic or prokaryotic cells (25).

For NGS, we used a Multiplicom Somatic 1 Master Kit manufactured for FFPE tumor tissue DNA analysis. To our best knowledge, this is the first study that uses the kit for ctDNA testing. We took into account similar properties of FFPE DNA and ctDNA. Clear and sensitive results were obtained from all the tested ctDNA specimens. The total number of plasma ctDNA mutated in *KRAS* or *BRAF* reached 19%; the concordance of the ctDNA with FFPE results was 86%. Similar discrepancies have been previously reported (14, 26, 27). A lower than expected frequency of the mutated tissue specimens (28) could be explained by the small number of specimens in the study, by the elevated mortality rate of the subjects with more aggressive types of mutations, or by other reasons. No mutations were found in the *NRAS* gene. This finding corresponds to the generally low prevalence of *NRAS* mutations in colon tumors (29).

A lot of somatic mutations exist in other genes (*PTEN*, *EGFR*, *PIK3CA*, *ERBB2*, *PIK3R1*, etc.) in colorectal cancer. Although commercial kits for NGS analysis are currently available, their clinical use for predictive testing is not yet obligatory. Similarly, the clinical importance of determining these mutations in ctDNA has not yet been demonstrated.

Conclusions

In conclusion, testing somatic mutations in ctDNA seems to be a promising tool to monitor dynamically changing genotypes of tumor cells circulating in the body, and causing disease relapse. The optimized process of ctDNA extraction should help to obtain more reliable data on *KRAS*, *BRAF*, *NRAS*, and several other genes when using NGS and/or other molecular techniques in patients with metastatic colorectal cancer. We believe that our work would contribute to better standardization of the pre-analytical phase of ctDNA analysis, and to a broader use of ctDNA in clinical practice.

Acknowledgements

The study was supported by the project MZ CR – RVO (FNHK, 00179906) of the Ministry of Health, Czech Republic, and by the projects PRVOUK P37/11 and P37/09 of the Charles University in Prague, Faculty of Medicine in Hradec Králové, Czech Republic.

References

1. Lo YM, Zhang J, Leung TN, Lau TK, Chang AM, Hjelm NM. Rapid clearance of fetal DNA from maternal plasma. Am J Hum Genet 1999; 64: 218–24.
2. Leon SA, Shapiro B, Sklaroff DM, Yaros MJ. Free DNA in the serum of cancer patients and the effect of therapy. Cancer Res 1977; 37: 646–50.
3. Lo YM, Corbetta N, Chamberlain PF, et al. Presence of fetal DNA in maternal plasma and serum. Lancet 1997; 350: 485–7.
4. Wagner J. Free DNA: new potential analyte in clinical laboratory diagnostics? Biochem Med 2012; 22: 24–38.
5. García Moreira V, Prieto García B, Baltar Martín JM, Ortega Suárez F, Alvarez FV. Cell-free DNA as a noninvasive acute rejection marker in renal transplantation. Clin Chem 2009; 55: 1958–66.
6. Saukkonen K, Lakkisto P, Pettilä V, et al. Cell-free plasma DNA as a predictor of outcome in severe sepsis and septic shock. Clin Chem 2008; 54: 1000–7.
7. Pathak AK, Bhutani M, Kumar S, Mohan A, Guleria R. Circulating cell-free DNA in plasma/serum of lung cancer patients as a potential screening and prognostic tool. Clin Chem 2006; 52: 1833–42.
8. Lecomte T, Berger A, Zinzindohoué F, et al. Detection of free-circulating tumor-associated DNA in plasma of colorectal cancer patients and its association with prognosis. Int J Cancer 2002; 100: 542–8.
9. Giacona MB, Ruben GC, Iczkowski KA, Roos TB, Porter DM, Sorenson GD. Cell-free DNA in human blood plasma: length measurements in patients with pancreatic cancer and healthy controls. Pancreas 1998; 17: 89–97.
10. Suzuki N, Kamataki A, Yamaki J, Homma Y. Characterization of circulating DNA in healthy human plasma. Clin Chim Acta 2008; 387: 55–8.
11. Danese E, Montagnana M, Minicozzi AM, et al. Real-time polymerase chain reaction quantification of free DNA in serum of patients with polyps and colorectal cancers. Clin Chem Lab Med 2010; 48: 1665–8.
12. Freidin MB, Freydina DV, Leung M, et al. Circulating tumor DNA outperforms circulating tumor cells for KRAS mutation detection in thoracic malignancies. Clin Chem 2015; 61: 1299–304.
13. Sorenson GD, Pribish DM, Valone FH, Memoli VA, Bzik DJ, Yao SL. Soluble normal and mutated DNA sequences from single-copy genes in human blood. Cancer Epidemiol Biomarkers Prev 1994; 3: 67–71.
14. Anker P, Lefort F, Vasioukhin V, et al. K-ras mutations are found in DNA extracted from the plasma of patients with colorectal cancer. Gastroenterology 1997; 112: 1114–20.
15. Dawson SJ, Tsui DW, Murtaza M, et al. Analysis of circulating tumor DNA to monitor metastatic breast cancer. N Engl J Med 2013; 368: 1199–209.
16. Albanese I, Scibetta AG, Migliavacca M, et al. Heterogeneity within and between primary colorectal carcinomas and matched metastases as revealed by analysis of Ki-ras and p53 mutations. Biochem Biophys Res Commun 2004; 325: 784–91.
17. Baldus SE, Schaefer KL, Engers R, Hartleb D, Stoecklein NH, Gabbert HE. Prevalence and heterogeneity of KRAS, BRAF, and PIK3CA mutations in primary colorectal adenocarcinomas and their corresponding metastases. Clin Cancer Res 2010; 16: 790–9.
18. Diaz LA Jr, Williams RT, Wu J, et al. The molecular evolution of acquired resistance to targeted EGFR blockade in colorectal cancers. Nature 2012; 486: 537–40.
19. Mouliere F, El Messaoudi S, Pang D, Dritschilo A, Thierry AR. Multi-marker analysis of circulating cell-free DNA toward personalized medicine for colorectal cancer. Mol Oncol 2014; 8: 927–41.
20. Mouliere F, Robert B, Arnau Peyrotte E, et al. High fragmentation characterizes tumour-derived circulating DNA. PLoS One 2011; 6: e23418.
21. Kirsch C, Weickmann S, Schmidt B, Fleischhacker M. An improved method for the isolation of free-circulating plasma DNA and cell-free DNA from other body fluids. Ann N Y Acad Sci 2008; 1137: 135–9.
22. Shaw KJ, Thain L, Docker PT, et al. The use of carrier RNA to enhance DNA extraction from microfluidic-based silica monoliths. Anal Chim Acta 2009; 652: 231–3.
23. Kishore R, Hardy R, Anderson VJ, Sanchez NA, Buoncristiani MR. Optimization of DNA extraction from low-yield and degraded samples using the BioRobot EZ1 and BioRobot M48. J Forensic Sci 2006; 51: 1055–61.
24. Cheung RC, Matsui SM, Greenberg HB. Rapid and sensitive method for detection of hepatitis C virus RNA by using silica particles. J Clin Microbiol 1994; 32: 2593–7.
25. Hengen PN. Carriers for precipitating nucleic acids. Trends Biochem Sci 1996; 21: 224–5.
26. Kopreski MS, Benko FA, Borys DJ, Khan A, McGarrity TJ, Gocke CD. Somatic mutation screening: identification of individuals harboring K-ras mutations with the use of plasma DNA. J Natl Cancer Inst 2000; 92: 918–23.
27. Ryan BM, McManus RO, Daly JS, et al. Serum mutant K-ras in the colorectal adenoma-to-carcinoma sequence. Implications for diagnosis, postoperative follow-up, and early detection of recurrent disease. Ann N Y Acad Sci 2000; 906: 29–30.
28. Andreyev HJ, Norman AR, Cunningham D, et al. Kirsten ras mutations in patients with colorectal cancer: the 'RASCAL II' study. Br J Cancer 2001; 85: 692–6.
29. De Roock W, Claes B, Bernasconi D, et al. Effects of KRAS, BRAF, NRAS, and PIK3CA mutations on the efficacy of cetuximab plus chemotherapy in chemotherapy-refractory metastatic colorectal cancer: a retrospective consortium analysis. Lancet Oncol 2010; 11: 753–62.

Received: 10/02/2016
Accepted: 18/04/2016

ORIGINAL ARTICLE

Effect of Intramuscular Injection on Oxidative Homeostasis in Laboratory Guinea Pig Model

Alžběta Kračmarová[1], Hana Banďouchová[2], Jiří Pikula[2], Miroslav Pohanka[3,]*

[1] Department of Toxicology and Military Pharmacy, Faculty of Military Health Sciences, University of Defence, Hradec Králové, Czech Republic
[2] Department of Ecology and Diseases of Game, Fish and Bees, Faculty of Veterinary Hygiene and Ecology, University of Veterinary and Pharmaceutical Sciences, Brno, Czech Republic
[3] Department of Molecular Pathology and Biology, Faculty of Military Health Sciences, University of Defence, Hradec Králové, Czech Republic
* Corresponding author: Faculty of Military Health Sciences, University of Defense, Brno, Třebešská 1575, 50001 Hradec Králové, Czech Republic; e-mail: miroslav.pohanka@gmail.com

Summary: In animal models, there was observed alteration of various physiological processes caused by microtraumas. Here reported experiment was aimed on the research of link between injection and development of an oxidative imbalance. Laboratory guinea pig was chosen as a suitable model for examining of the oxidative stress.
Markers indicating oxidative homeostasis were assayed in the frontal, temporal and occipital brain lobe, cerebellum, liver, kidney, spleen and heart one hour after an intramuscular injection. Common biochemical parameters were measured in plasma samples as well.
The most extensive effect was observed in the heart where the thiobarbituric acid reactive substances value was more than twice increased after the injection. The level of carbonylated proteins was significantly elevated in the kidney and ferric reducing antioxidant power value was increased in the brain compartments. The enzyme activities in the organs were not influenced except the activity of superoxide dismutase, which was moderately decreased in the brain. In the plasma samples, there was observed increase of the blood urea nitrogen.
The results showed significant the influence of the intramuscular injection on a development of an oxidative insult. The injection can be considered as an adverse effect with quite extensive stress consequences.

Keywords: *Injection; Oxidative stress; Antioxidant; Microtrauma; Animal model*

Introduction

Owing to many scientific reports, oxidative stress plays an important role in pathogenesis of various diseases (neurodegenerative disorders, cardiovascular diseases, cancer), in the processes linked to ageing and in adverse effects of some drugs (1–4). Ferric reducing antioxidant power (FRAP), thiobarbituric acid reactive substances (TBARS), carbonylated proteins, superoxide dismutase (SOD) activity and glutathione reductase (GR) activity are markers indicating oxidative stress and oxidative homeostasis (5). The markers are often used for demonstration of detrimental or beneficial effects of various substances to laboratory animal models (6–8).

Guinea pig (*Cavia porcellus*) is not able to synthesize ascorbic acid, which ranks among the most important low molecular weight antioxidants. That is the main reason why guinea pig is widely used laboratory model for examining of the oxidative stress (9–11). The inability to produce endogenous ascorbic acid makes results from guinea pigs extrapolatable to humans (12–14). Except the inability to synthesize vitamin C there are other similarities like a similar response of lipid metabolism to dietary intervention (15).

Small rodents, including guinea pigs, are very sensitive to a way of handling and to living conditions. Stress caused by manipulation or inconvenient housing may lead to alteration of results in separate experiments. E. g., presence or an absence of huts can significantly influent a level of stress hormones in laboratory guinea pig (16).

However, psychical stress affects more processes than the secretion of stress hormones. In laboratory animals, experimentally induced stress elicits tachycardia and rise of body temperature (17, 18). Transient increase of body temperature after a stress stimulus is called stress-induced hyperthermia and it was observed in multiple laboratory animals. Measuring of the stress induced hyperthermia is a standard test for recognizing psychical stress in animals. After injection, a complication for example in testing of anxiolytic drugs was observed (19, 20). Alteration of various physiological processes caused by the injection stress was

http://dx.doi.org/10.14712/18059694.2016.90

noticed in small laboratory rodents. Renaud et al. (21) observed facilitation of learning caused by adolescent injection stress in laboratory rat model. On the other hand, no significant alterations in behavior and in hematologic parameters and no elevation of fecal corticosterone level were found in mice undergoing multiple intraperitoneal injections (22).

Despite knowledge about injection stress, studies focused on the implication of the injection in the oxidative homeostasis have not been done yet. The objective of our experiment was to confirm or exclude implication of intramuscular injection (which is a common way of drug administration in experiments on laboratory animal models) in the markers of oxidative stress levels.

Material and methods

Animal exposure, sample collecting and sample preparation

The experiment was permitted and supervised by the Ethical Committee of the Faculty of Military Health Sciences, University of Defence, Hradec Králové, Czech Republic.

The male guinea pigs were purchased from the Velaz Company (Prague, Czech Republic). They were at the age of three months and their body weight was 250 ± 10 g. The animals were kept in the experimental facility (22 ± 2 °C, 50 ± 10% humidity, 12 hours light period per a day) and they were fed by a common food, supplemented with vitamins including vitamin C, and water *ad libitum*.

The guinea pigs were divided into two groups – injection and control group. Each group consisted of eight specimens. The saline solution in the amount of 100 µl per 100 g of body weight was intramuscularly injected into the pelvic limb of the animal in the injection group. The animals in the control group were exposed to the manual handling imitating the condition of the injection.

At the time of 1 hour after the injection, the animals were sacrificed in CO_2. The blood was collected by cutting carotide into tubes with lithium heparine and centrifuged at 1,000 × g. Separated plasma was transferred into a new tube, frozen immediately and stored at −80 °C. In a total, the liver, kidney, spleen, heart, cerebellum, frontal, temporal and occipital lobe were collected. After the collection, 100 mg of the tissue was mixed with 1 ml of phosphate buffer saline (Sigma-Aldrich, Saint Louis, USA) and mechanically homogenized by an Ultra-Turrax mill (Ika Werke, Staufen, Germany) for one minute. The homogenates were frozen immediately and stored at –80 °C as well.

Markers of oxidative stress and biochemical markers assessment

FRAP, TBARS, carbonylated proteins, caspase 3 (CASP3), SOD and GR were measured in tissue homogenates and levels of glucose, total cholesterol, HDL cholesterol, triglycerides (TG), blood urea nitrogen (BUN), creatinine (CRE), total bilirubin, total protein, albumin and activities of aspartate aminotransferase (AST), alanine aminotransferase (ALT), alkaline phosphatase (ALP) and lactate dehydrogenase (LDH) were measured in plasma samples.

FRAP is a spectrophotometric method based on reduction of ferric to ferrous ions. Concentration of malondialdehyde was assayed as TBARS by spectrophotometry using thiobarbituric acid. The FRAP and TBARS were done in compliance with reported paper (23). Carbonylated proteins were measured according to the protocol published by Cao & Cutler (24) with minor modifications which are mentioned in references (23). 2,4,6-Tris(2-pyridyl)-S-triazine, ferric chloride (Sigma-Aldrich, Saint Louis, USA) were purchased for FRAP, dimethylsulfoxide, trichloroacetic acid and thiobarbituric acid (Sigma-Aldrich) for TBARS and 2,4-dinitrophenylhydrazine, trichloracetic acid (Sigma-Aldrich), hydrochloric acid, ethanol and ethyl acetate (Penta, Prague, Czech Republic) for the assay of protein carbonyls.

The GR activity was measured as the Wartburg optical test. The assay was performed as described previously (25). Oxidized glutathione, NADPH, ethylenediaminetetraacetic acid disodium salt dihydrate (Sigma-Aldrich) and phosphate buffer saline were purchased for the measurement. For the SOD and CASP3 activity assessment, the Sigma caspase 3 assay kit and the SOD assay kit (Sigma-Aldrich) were used. The SOD activity in the tissue homogenates was quite high, so it was need for dissolving the samples.

Biochemical parameters in plasma were assessed using an automated analyzer SPOTCHEM TM EZ SP-4430 (Arkray, Japan).

Statistical evaluation

Comparison of the data obtained from the control and injection group was done using one-way ANOVA with Bonferroni test (or Bonferroni correction in some sources). The analysis was processed using the statistical software Origin 8 SR2 (OriginLab Corporation, Northampton, USA).

Results

The most extensive effect of the injection on stress markers was observed in the heart where the TBARS value was more than twice increased 1 hour after the injection. However, no significant alterations of the TBARS value were found in the other organs. The level of carbonylated proteins was significantly elevated in the kidney one hour after the injection. On the other hand, the other organs had insignificant alteration in the level of protein carbonyls.

The FRAP value was significantly increased in the frontal lobe and in the cerebellum one hour after the injection. In the spleen, there was increased FRAP value as well. However, the increase was not significant. In the other organs including the temporal and occipital lobe, only slight changes in the FRAP value were observed.

Activities of the enzymatic markers in the tissue homogenates were quite stable. One exception was in the temporal and occipital lobe where moderate and statistically significant decrease of the SOD activity was proved. The CASP3 activity in the heart and in all of the brain compartments was too low for measurement by the assay. In other organs, we did not notice any significant change of the CASP3 activity.

In the plasma samples, levels of total and HDL cholesterol forms and creatinine were not detectable (total cholesterol bellow 1.3 mmol/l, HDL cholesterol bellow 0.26 mmol/l and creatinine bellow 27 µmol/l). Biochemical test proved statistically significant alteration in BUN level. The marker was elevated from 4.78 ± 0.29 mmol/l (control group) to 7.92 ± 0.44 mmol/l (1 hour after the injection). The other

Tab. 1: Ferric reducing antioxidant power (FRAP), thiobarbituric acid reactive substances (TBARS) and carbonylated proteins in tissue samples ± standard errors of mean.

Assay	FRAP [µmol/g]		TBARS [µmol/g]		carbonylated proteins [µmol/g]	
	control	injection	control	injection	control	injection
liver	2.58 ± 0.14	1.86 ± 0.31	0.177 ± 0.007	0.185 ± 0.017	0.323 ± 0.008	0.362 ± 0.033
kidney	1.96 ± 0.14	1.84 ± 0.20	0.240 ± 0.018	0.205 ± 0.007	0.259 ± 0.015	0.327 ± 0.006**
spleen	1.90 ± 0.12	2.45 ± 0.19	0.102 ± 0.012	0.0732 ± 0.0085	0.249 ± 0.020	0.235 ± 0.018
heart	0.376 ± 0.017	0.484 ± 0.062	0.0738 ± 0.0036	0.189 ± 0.008**	0.266 ± 0.019	0.249 ± 0.020
frontal lobe	0.262 ± 0.015	0.336 ± 0.007**	0.295 ± 0.013	0.291 ± 0.007	0.249 ± 0.017	0.269 ± 0.010
temporal lobe	0.260 ± 0.016	0.273 ± 0.013	0.305 ± 0.015	0.323 ± 0.017	0.284 ± 0.018	0.228 ± 0.022
occipital lobe	0.225 ± 0.011	0.215 ± 0.025	0.253 ± 0.012	0.261 ± 0.011	0.253 ± 0.011	0.257 ± 0.015
cerebellum	0.184 ± 0.013	0.252 ± 0.005*	0.273 ± 0.013	0.292 ± 0.027	0.256 ± 0.015	0.265 ± 0.015

* $p < 0.05$, ** $p < 0.01$, n = 8 specimens in each group

Tab. 2: Glutathione reductase (GR), superoxide dismutase (SOD) and caspase 3 (CASP3) in tissue samples ± standard errors of mean.

assay	GR [nkat/g]		SOD [nkat/g]		CASP3 [pkat/g]	
	control	injection	control	injection	control	injection
liver	103 ± 7	126 ± 4	275 ± 0	274 ± 0	52.8 ± 7.1	46.0 ± 4.1
kidney	115 ± 5	116 ± 3	267 ± 1	267 ± 2	28.1 ± 4.1	26.8 ± 4.1
spleen	53.5 ± 4.8	76.2 ± 3.8	206 ± 3	208 ± 3	69.4 ± 14.9	62.4 ± 8.8
heart	18.0 ± 0.9	17.9 ± 2.2	161 ± 3	161 ± 5		
frontal lobe	63.4 ± 2.8	66.2 ± 5.4	205 ± 2	200 ± 4		
temporal lobe	62.4 ± 7.8	62.5 ± 4.1	216 ± 4	196 ± 5**		
occipital lobe	68.7 ± 8.9	57.8 ± 4.6	205 ± 2	188 ± 7**		
cerebellum	42.0 ± 5.9	62.0 ± 7.8	232 ± 2	223 ± 2		

** $p < 0.01$, n = 8 specimens in each group

Tab. 3: Biochemical marker assesment in plasma samples ± standard errors of mean. Abbreviations used in the table: AST – aspartate aminotransferase; ALT – alanine aminotransferase; LDH – lactate dehydrogenase; ALP – alkaline phosphatase; BUN – blood urea nitrogen; T-pro – total plasma protein; Alb – albumin; T-bil – total bilirubin; TG – triglycerides; GLU – glucose.

Assay	Control	Injection	Assay	Control	Injection
AST [µkat/l]	2.03 ± 0.35	1.31 ± 0.41	T-Pro [g/l]	39.8 ± 0.8	44.2 ± 2.0
ALT [µkat/l]	0.738 ± 0.064	0.817 ± 0.061	Alb [g/l]	20.7 ± 0.2	20.7 ± 1.3
LDH [µkat/l]	12.1 ± 3.45	4.88 ± 1.25	T-Bil [µmol/l]	5.67 ± 0.33	5.67 ± 1.28
ALP [µkat/l]	5.39 ± 0.47	4.25 ± 0.22	TG [mmol/l]	0.403 ± 0.081	0.362 ± 0.041
BUN [mmol/l]	4.78 ± 0.29	7.92 ± 0.44**	GLU [mmol/l]	9.02 ± 0.18	7.83 ± 0.25

** $p < 0.01$, n = 8 specimens in each group biochemical markers assessed in the plasma were altered in a very low scale, except the AST and LDH activity, which were quite noticeably but not significantly declined – AST from 2.03 ± 0.35 µkat/l (control group) to 1.31 ± 0.41 µat/l (1 hour after the injection) and LDH from 12.1 ± 3.45 µkat/l (control group) to 4.88 ± 1.25 µkat/l (1 hour after the injection). Experimental data are summarized in tables 1 (oxidative stress markers), 2 (specific enzymatic markers) and 3 (biochemical markers).

Discussion

The TBARS value informs about a level of malondialdehyde which signifies lipid peroxidation and so oxidative damage of cell membranes (6, 26–28). In a similar way, protein carbonyls are products of an irreversible oxidative modification of proteins (6, 26, 29, 30). From the elevated TBARS value in the heart and the content of carbonylated proteins in the kidney of guinea pigs exposed to the injection stress, we can infer that the heart and kidney tissue were injured by the oxidative stress. These findings are in compliance with the observation of Reis et al. (31), who stated that psychical stress can contribute to the elevation of reactive oxygen, nitrogen and sulphur levels in the laboratory guinea pig model. However, other tissues seem to be more resistant to oxidative stress.

FRAP level corresponds to the concentration of the low molecular weight antioxidants (9). As the FRAP level was elevated, we judge that the injection stress caused activation of the antioxidant system in the cerebellum and the in the frontal lobe.

GR and SOD are enzymes participating in the antioxidant defense of the organism. GR catalyzes regeneration of reduced glutathione from its oxidized form. The task of SOD is to accelerate the transformation of superoxide anion, into hydrogen peroxide. Their increased activity occurs when the oxidative stress in the organism rises. On the other hand, when the oxidative stress is too high and the capacity of the antioxidant system is depleted, the activity of SOD and GR can decrease as well (6). We found slightly decreased SOD activity in the temporal and the occipital lobe. The results were quite surprising, because no other marker signs the oxidative stress exceeding the capacity of the antioxidant system in the temporal and occipital lobe. For the reason, depletion in the SOD level is not well understood.

CASP3 is an enzyme participating in the apoptotic cascade. Its activation is, besides other processes, directly linked to the oxidative stress caused by mitochondrial failure (32). As the CASP3 activity was not elevated in any of the examined organ, we infer that injection stress did not lead to the apoptosis.

The results of the plasma biochemical markers` assay were influenced by the injection stress as well. The BUN level was nearly twice increased one hour after the injection. The similar effect is often described in relation to the muscle injury caused by the intramuscular injection (33), to the kidney malfunction (34) or to the acute-phase proteins production (35). Owing to the selected biochemical markers indicating tissue damage, we demonstrated that the micro-traumatic injury probably does not play a crucial role as both AST and LDH were not increased. Unfortunately, the assays were followed by quite extensive differences indicating high inter-individual variability. If the muscle is serious injured by the injection, the LDH activity will raise. The kidney is relatively susceptible to the oxidative damage which can be manifested by the increase of BUN (36). As was mentioned above, the kidneys of the animals in the injection group showed a marker of the oxidative injury (increased level of protein carbonyls in comparison to the control group). For the reason, the increase of the BUN level is probably linked to the oxidative kidney injury caused by the injection stress.

Rabe (37) established reference ranges for blood chemistry in guinea pigs by the use of a common dry chemistry blood analyzer. Considering the fact, that another analyzer was used for the measurement, the levels of biochemical markers found in the injection as well as the control group corresponded with the published data. Even the described BUN alteration did not deviate from the reference range. However, the difference between groups in BUN level is evaluated as statistically significant.

As was described previously, drug application using an injection is a very stressful moment for small laboratory rodents and the injection stress may alter a homeostasis of an experimental organism in a multiple way (19–21, 38). Our results show, that the oxidative homeostasis could be altered after the injection. The imbalance in oxidative homeostasis is higher when compared to the direct tissue damage indicated by the biochemical markers LDH and AST. Considering extrapolation of the results on humans, we can expect that repeated application of a drug using injection would initiate an oxidative insult even without a manifestation in standard biochemical markers.

In a conclusion, we proved significant link of injection on a development of an oxidative insult. Separate organs can be burdened by an oxidative stress insult shortly after an injection administration. The findings are in compliance with the other experimental works, as mentioned in the introduction. For the reason, it is always necessary to inject an appropriate volume of saline solution or similar solution to animals belonging to a control group. Moreover, the injection can be considered as an insult with quite extensive stress consequences.

Acknowledgements

University of Veterinary and Pharmaceutical Sciences Brno, Czech Republic, and University of Defense, Czech Republic (A long-term organization development plan 1011) are gratefully acknowledged for institutional support.

References

1. Thomas RR, Khan SM, Smigrodzki RM, et al. RhTFAM treatment stimulates mitochondrial oxidative metabolism and improves memory in aged mice. Aging 2012; 4(9): 620–35.
2. Valenzuela R, Khan SM, Smigrodzki RM, et al. N-3 long-chain polyunsaturated Fatty Acid supplementation significantly reduces liver oxidative stress in high fat induced steatosis. PLoS One 2012; **7**(10): e46400.
3. Baierle M, Nascimento SN, Moro AM, et al. Relationship between inflammation and oxidative stress and cognitive decline in the institutionalized elderly. Oxid Med Cell Longev 2015; 2015: 804198.
4. Chin-Chan M, Navarro-Yepes J, Quintanilla-Vega B. Environmental pollutants as risk factors for neurodegenerative disorders: Alzheimer and Parkinson diseases. Front Cell Neurosci 2015; 9: 124.
5. Miller LE, McGinnis GR, Kliszczewicz B, et al. Blood oxidative stress markers during a high altitude trek. Int J Sport Nutr Exerc Metab 2013; 23(1): 65–72.
6. Prasad SN, Muralidhara. Evidence of acrylamide induced oxidative stress and neurotoxicity in Drosophila melanogaster – Its amelioration with spice active enrichment: Relevance to neuropathy. Neurotoxicol 2012; 33(5): 1254–64.
7. Erman H, Guner I, Yaman MO, et al. The effects of fluoxetine on circulating oxidative damage parameters in rats exposed to aortic ischemia–reperfusion. Eur J Pharmacol 2015; 749: 56–61.
8. Hagar H, El Medany A, Salamb R, El Medany G, Nayal OA. Betaine supplementation mitigates cisplatin-induced nephrotoxicity by abrogation of oxidative/nitrosative stress and suppression of inflammation and apoptosis in rats. Exp Toxicol Pathol 2015; 67: 133–41.
9. Pohanka M, Hrabinova M, Zemek F, Drtinova L, Bandouchova H, Pikula J. Huperzine induces alteration in oxidative balance and antioxidants in a guinea pig model. Neuro Endocrinol Lett 2011; 32(suppl.): 95–100.
10. Al-Hasan YM, Evans LC, Pinkas GA, Dabkowski ER, Stanley WC, Thompson LP. Chronic hypoxia impairs cytochrome oxidase activity via oxidative stress in selected fetal guinea pig organs. Reprod Sci 2012; 20(3): 299–307.
11. Xie C, Kauffman J, Akar FG. Functional crosstalk between the mitochondrial PTP and KATP channels determine arrhythmic vulnerability to oxidative stress. Front Phisiol 2014; 5: 264.
12. Kim JCS. Ultrastructural studies of vascular and muscular changes in ascorbic acid deficient guinea-pigs. Lab Anim 1977; 11(2): 113–7.
13. Das A, Dey N, Ghosh A, Das S, Chattopadhyay DJ, Chatterjee IB. Molecular and cellular mechanisms of cigarette smoke-induced myocardial injury: Prevention by vitamin C. PLoS One 2012; **7**(9): e44151.
14. Paidi MD, Schjoldager JG, Lykkesfeldt J, Tveden-Nyborg P. Prenatal vitamin C deficiency results in differential levels of oxidative stress during late gestation in foetal guinea pig brains. Redox Biol 2014; 2: 361–7.
15. Kim JE, Clark RM, Park Y, Lee J, Fernandez ML. Lutein decreases oxidative stress and inflammation in liver and eyes of guinea pigs fed a hypercholesterolemic diet. Nutr Res Pract 2012; 6(2): 113–9.
16. Walters SL, Torres-Urbano CJ, Chichester L, Rose RE. The impact of huts on physiological stress: a refinement in post-transport housing of male guinea pigs (Cavia porcellus). Lab Anim 2012; 46(3): 220–4.
17. Pattij T, Groenink L, Hijzen TH, et al. Autonomic changes associated with enhanced anxiety in 5-HT1A receptor knockout mice. Neuropsychopharmacol 2002; 27(3): 380–90.
18. Thompson T, Grabowski-Boase L, Tarantino LM. Prototypical anxiolytics do not reduce anxiety-like behavior in the open field in C57BL/6J mice. Pharmacol Biochem Behav 2015; 133: 7–17.
19. Vinkers CH, van Bogaert MJV, Klanker M, et al. Translational aspects of pharmacological research into anxiety disorders: The stress-induced hyperthermia (SIH) paradigm. Eur J Pharmacol 2008; 585: 407–25.
20. Vinkers CH, de Jong NM, Kalkman CJ, et al. Stress-induced hyperthermia is reduced by rapid-acting anxiolytic drugs independent of injection stress in rats. Pharmacol Biochem Behav 2009; 93: 413–8.
21. Renaud SM, Pickens LRG, Fountain SB. Paradoxical effects of injection stress and nicotine exposure experienced during adolescence on learning in a serial multiple choice (SMC) task in adult female rats. Neurotoxicol Teratol 2015; 48: 40–8.
22. Davis JN, Courtney CL, Superak H, Taylor DK. Behavioral, clinical and pathological effects of multiple daily intraperitoneal injections on female mice. Lab Anim (NY) 2014; 43(4): 131–9.
23. Pohanka M, Sobotka J, Jilkova M, Stetina R. Oxidative stress after sulfur mustard intoxication and its reduction by melatonin: efficacy of antioxidant therapy during serious intoxication. Drug Chem Toxicol 2010; 34: 85–91.
24. Cao G, Cutler RG. Protein oxidation and aging. Arch Biochem Biophys 1995; 320: 106–14.
25. Pohanka M, Sobotka J, Stetina R. Sulfur mustard induced oxidative stress and its alteration by epigallocatechin gallate. Toxicol Lett 2011; 201: 105–9.
26. Subramanian K, Mohideen SS, Suzumura A, et al. Exposure to 1-bromopropane induces microglial changes and oxidative stress in the rat cerebellum. Toxicology 2012; 302(1): 18–24.
27. Oleszko A, Olsztyńska-Janus S, Walski T, et al. Application of FTIR-ATR spectroscopy to determine the extent of lipid peroxidation in plasma during haemodialysis. Biomed Res Int 2015; 2015: 245607.
28. Yi G, Grabež V, Bjelanovic M, et al. Lipid oxidation in minced beef meat with added Krebs cycle substrates to stabilise colour. Food Chem 2015; 187: 563–71.
29. Berardo A, Claeys E, Vossena E, Leroy F, De Smet S. Protein oxidation affects proteolysis in a meat model system. Meat Sci 2015; 106: 78–84.
30. Wang Z, Wang Y, Liu H, Che Y, Xu Y, E L. Age-related variations of protein carbonyls in human saliva and plasma: is saliva protein carbonyls an alternative biomarker of aging? Age 2015; 37: 48.
31. Reis FG, Marques RH, Starling CM, et al. Stress amplifies lung tissue mechanics, inflammation and oxidative stress induced by chronic inflammation. Exp Lung Res 2012; 38(7): 344–54.
32. Zhu Y, Li M, Wang X, et al. Caspase cleavage of cytochrome c1 disrupts mitochondrial function and enhances cytochrome c release. Cell Res 2012; 22(1): 127–41.
33. Lee BR, Lee JH, An HJ. Effects of Taraxacum officinale on fatigue and immunological parameters in mice. Molecules 2012; 17: 13253–65.
34. El-Naga RN. Pre-treatment with cardamonin protects against cisplatin-induced nephrotoxicity in rats: Impact on NOX-1, inflammation and apoptosis. Toxicol Appl Pharmacol 2014; 274: 87–95.
35. Thomsen KL. Regulation of urea synthesis during the acute phase response in rats. Dan Med J 2013; 60(4): B461.
36. Singh JP, Singh AP, Bhatti R. Explicit role of peroxisome proliferator-activated receptor gamma in gallic acid-mediated protection against ischemia-reperfusion-induced acute kidney injury in rats. J Surg Res 2014; 187(2): 631–9.
37. Rabe H. [Reference ranges for biochemical parameters in guinea pigs for the Vettest®8008 blood analyzer. (In German with English abstract)] Tierarztl Prax Ausg K Kleintiere Heimtiere 2011; 39(3): 170–175.
38. Kim DH, Jung JS, Moon YS, et al. Inhibition of intracerebroventricular injection stress-induced plasma corticosterone levels by intracerebroventricularly administered compound K, a Ginseng saponin metabolite, in mice. Biol Pharm Bull 2003; 26(7): 1035–8.

Received: 19/01/2016
Accepted: 07/04/2016

CASE REPORT

Transient Splenial Lesion of the Corpus Callosum Related to Migraine with Aura in a Pediatric Patient

Olcay Ünver, MD[1,], Büşra Kutlubay, MD[1], Tolga Besci, MD[2], Gazanfer Ekinci, MD[3], Feyyaz Baltacıoğlu, MD[3], Dilşad Türkdoğan, MD[3]*

[1] Department of Pediatric Neurology, Marmara University, İstanbul, Turkey
[2] Department of Pediatrics, Marmara University, İstanbul, Turkey
[3] Department of Radiology, Marmara University, İstanbul, Turkey
* Corresponding author: Marmara University Fevzi Çakmak Mah. Muhsin Yazıcıoğlu Cad. No: 10 Üst, Kaynarca / Pendik / İstanbul, Turkey; e-mail: olcaymd@hotmail.com

Summary: Background: Transient splenial lesions of the corpus callosum are rare radiological findings first described in association with epilepsy, antiepileptic drugs and viral encephalitis. However, subsequently more cases were described associated with diverse clinical conditions. Case report: We describe a 13-year-old girl suffering from migraine with aura presenting with headache, right-sided hemiparesis and encephalopathy. Brain magnetic resonance imaging revealed an ovoid lesion in the splenium of the corpus callosum. The patient's neurological symptoms resolved within 3 days without therapy and the lesion disappeared in follow up magnetic resonance images obtained 3 weeks after the onset of the symptoms. Results: Migraine with aura was considered to be the cause of the lesion. To our knowledge the present case is the first report of a pediatric patient with a diagnosis of migraine with aura presenting with hemiparesis and encephalopathy. Conclusions: A diagnosis of transient lesion of the corpus callosum should be suspected in patients with migraine with aura presenting with hemiparesis and encephalopathy. A mild course and a good prognosis might be expected in the presence of a splenial lesion of the corpus callosum.

Keywords: *Transient splenial lesion; Corpus callosum; Migraine with aura; Encephalopathy; Hemiparesis*

Introduction

Transient splenial lesions of the corpus callosum are described in association with many diverse clinical conditions including various infections, use or withdrawal of antiepileptic drugs, and hypoglycemia (1–6). The lesion appears as a well-defined hyperintense ovoid lesion in the center of the splenium of the corpus callosum, best observed in diffusion weighted brain magnetic resonance images. The pathology is unclear as well as the specific location of the lesion. This new clinico-radiological entity presents with mild encephalitis/encephalopathy in clinical practice (2). The usual clinical manifestations include disturbance of consciousness, delirium, seizures and headache, which resolve in a couple of days. The lesion itself also disappears in follow-up radiological images (1, 2).

Here we present a pediatric case with a transient splenial lesion of the corpus callosum related to migraine with aura. To our knowledge our patient is the first pediatric case of transient splenial lesion of the corpus callosum related to migraine with aura presenting with encephalopathy and hemiparesis.

Case report

A 13-year old girl was admitted with a severe headache, confusion, violent behavior, slurred speech, and right-sided hemiparesis. She first experienced similar but milder attacks of a throbbing headache accompanied by nausea and vomiting following numbness feeling in the lips and slurred speech, which had lasted for 2–3 hours and not complicated with hemiparesis, two months before. At the time, brain magnetic resonance imaging (MRI) and electroencephalography (EEG) were unremarkable. After checking family history it was learned that her mother and her aunt suffer from migraine and the diagnosis of migraine with aura was made according to the criteria of International Classification of Headache Disorders two months before (7). Her parents stated that this last attack was the worst one and the symptoms lasted longer and complicated with loss of muscle strength, personality changes and violent behavior. On admission she was confused. On physical examination she was afebrile. Neurological examination was otherwise unremarkable except for 4/5 muscle strength on the right side of her body. Routine laboratory tests including complete blood count, biochemistry, electrolytes, prothrombin time and partial

ACTA MEDICA (Hradec Králové) 2016; 59(2):64–66
http://dx.doi.org/10.14712/18059694.2016.91

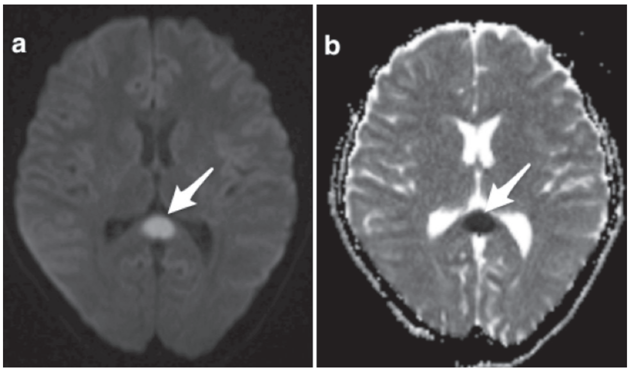

Fig. 1: Transient splenial lesion in a pediatric patient suffering from migraine with aura. An axial diffusion weighted magnetic resonance image shows a hyperintense lesion in the splenium of the corpus callosum (a) and corresponding hypointense lesion in apparent diffusion coefficient images (b).

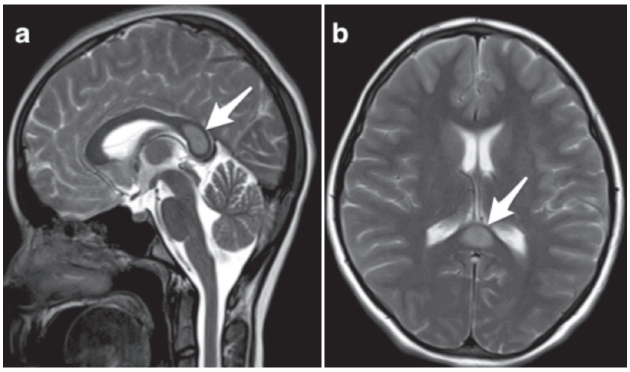

Fig. 2: Transient splenial lesion in a pediatric patient suffering from migraine with aura in a sagittal T2 weighted image (a) and in an axial T2 weighted image (b).

thromboplastin time were all normal. C-reactive protein and erythrocyte sedimentation rate were within normal limits. Serum antibody titers to Epstein-Barr virus, Cytomegalovirus, Hepatitis B and C virus and Varicella Zoster virus, Parvovirus B19, Mycoplasma pneumonia, Legionella pneumophila, Chlamydia pneumonia were all normal. A lumbar puncture revealed a normal opening pressure, a normal leucocyte count and normal glucose and protein levels. Brain MRI conducted that day revealed a well-circumscribed ovoid lesion in the splenium of the corpus callosum, hyperintense in diffusion-weighted magnetic resonance images and hypointense in apparent diffusion coefficient images (Figure 1a,b). The lesion exhibited moderate hyperintensity in T2 weighted images (Figure 2a,b). No enhancement was evident after gadolinium administration. Her EEG revealed generalized, high amplitude intermittent slow delta waves prominent on frontal areas, which is consistent with encephalopathy (Figure 3a). Neurological examination revealed normal results about 36 hours after the first neurological symptoms. Follow-up EEG on day 3 showed significant

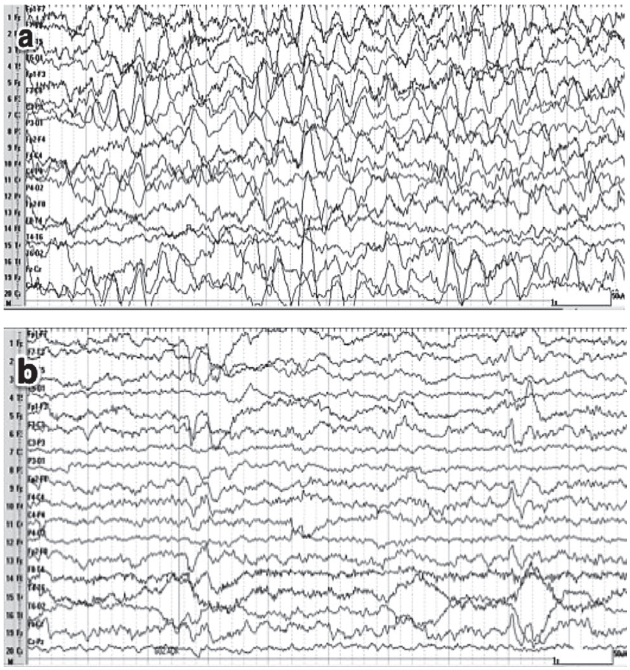

Fig. 3: Electroencephalography of the patient. Global diffuse waves prominent on the frontal areas consistant with encephalopathy (a). İmprovement of EEG after 3 days (b).

improvement (Figure 3b). She was discharged 4 days after admission with a completely normal neurological examination. Her follow-up MRI 3 weeks after the first MRI, revealed a complete disappearance of the lesion.

Discussion

We reported an unusual case of transient splenial lesion of the corpus callosum presenting with encephalopathy and right-sided hemiparesis related to migraine with aura in a pediatric patient. In recent years, a uniform temporary lesion confined only to the splenium of the corpus callosum has been repeatedly reported (1, 3, 8). The typical presentation is a well defined ovoid lesion in the center of the corpus callosum, which is hyperintense on T2 weighted images iso- or hypointense on T1 weighted images with no evidence of contrast enhancement and best observed on diffusion weighted images with low apparent diffusion coefficient values, which indicates restricted diffusion (9). To our knowledge 2 cases of migraine with aura as an associated condition have been reported to date. One of them is an adult patient with sensory aura (9) and the other a 17-year old girl with acephalgic migraine with a visual aura triggered by stimulant containing diet pills (10). None of these two patients presented with encephalitis or hemiparesis.

In a study where 5 patients with transient splenial lesion of the corpus callosum associated with influenza virus infection were presented, one patient had motor deficits explained by additional white matter lesions (3). In another report, an adult case related to adenovirus infection had right hemiparesis and hemianesthesia; however, no white matter lesions were detected on MRI images (4). The authors have two hypotheses; either a culprit lesion located within the deep white matter above the midbrain, which is not detectable on MRI images or the splenial lesion itself is responsible for the motor and sensory deficit. The authors support the first hypothesis based on the neuroanatomical localization of the lesion; however, they also state that the second option cannot be ruled out entirely, because of a previous report, which described corpus callosum body as being responsible for hemiparesis (11).

The exact pathology of the lesion is still unclear. Until today, many hypotheses have been described to explain the pathophysiology of the splenial lesion such as reversible demyelination probably due to antiepileptic drug toxicity or abrupt stoppage of chronic antiepileptic therapy, which could lead to ischemia and resultant cytotoxic edema (12, 13). Additionally, extrapontine osmotic myelinolysis due to sodium and glucose imbalance, and direct viral invasion have been held responsible for the lesion (14). However, most of the authors support that intramyelinic edema from the separation of myelin layers and inflammatory infiltrate rather than a breakdown of the blood brain barrier or demyelination are responsible for the lesion (1, 3), which explains the reversibility of the diffusion restriction of the lesion. Similarly, the reason for the specific predilection for the splenium of the corpus callosum has not been clarified yet (3).

All the patients' symptoms resolve invariably in a couple of days and the lesion disappears in follow-up MRI studies performed from 3 days to 3 months (15). To our knowledge, the lesion was detected only in 1 case in T2 weighted images over 5 months although decreased in size indicating that it could result in gliosis (15).

Conclusion

Clinicians should consider transient splenial lesion of corpus callosum in children with known migraine presenting with headache, encephalopathy and hemiparesis. A mild course and a good prognosis might be expected based on the reports to date.

References

1. Tada H, Takanashi J, Barkovich AJ, et al. Clinically mild encephalitis/encephalopathy with a reversible splenial lesion. Neurology 2004; 63:1854–8.
2. Takanashi J. Two newly proposed infectious encephalitis/encephalopathy syndromes. Brain Dev 2009; 31: 521–8.
3. Bulakbaşı N, Kocaoğlu, Tayfun C, Uçoz T. Transient splenial lesion of the corpus callosum in clinically mild influenza associated encephalitis/encephalopathy. Am J Neuroradiol 2006; 27: 1983–6.
4. Hibino M, Horiuchi S, Okubo Y, Kakutani T, Ohe M, Kondo T. Transient hemiparesis and hemianesthesia in an atypical case of adult-onset clinically mild encephalitis/encephalopathy with a reversible splenial lesion associated with adenovirus infection. Intern Med 2014; 53: 1183–5.
5. Meleková A, Andrlová L, Král P, Ungermann L, Ehler E. Encephalitis with Prolonged but Reversible Splenial Lesion. Acta Medica (Hradec Králové) 2015; 58(3): 108–12.
6. Degirmenci E, Degirmenci T, Cetin EN, Kıroğlu Y. Mild encephalitis/encephalopathy with a reversible splenial lesion (MERS) in a patient presenting with papilledema. Acta Neurol Belg. 2015 Jun; 115(2): 153–5.
7. Headache Classification Subcommitte of the International Headache Society. The International classification of headache disorders: 2nd edition. Cephalgia 2004; 24(suppl 1): 9–160.
8. Matsubara K, Kodera M, Nigami H, Yura K, Fukaya T. Reversible lesion in influenza virus encephalopathy. Pediatr Neurol 2007; 37: 431–4.
9. Yang CY, Lin FY. Reversible splenial lesion of the corpus callosum in migraine with aura. The Neurologist 2011; 17: 157–9.
10. Wislow H, Mickey B, Frohman EM. Sympathomimetic-induced kaleidoscopic visual illusion associated with a reversible splenium. Arch Neurol 2006; 63: 135–7.
11. Jang SH, Lee J, Yeo SS, Chang MC. Callosal disconnection syndrome after corpus callosum infarct: a diffusion tensor tractography study. J Stroke Cerebrovasc Dis 2013; 22: e240-e4.
12. Kim SS, Chang KH, Kim ST, et al. Focal lesion in the splenium of the corpus callosum in epileptic patients: Antiepileptic drug toxicity? Am J Neuroradiol 1999; 20: 125–9.
13. Gürtler S, Ebner A, Tuxhorn I, Ollech I, Pohlmann-Eden B, Woermann FG. Transient lesion in the splenium of the corpus callosum and antiepileptic drug withdrawal Neurology 2005; 65: 1032–6.
14. Polster T, Hoppe M, Ebner A. Transient lesion in the splenium of corpus callosum: three further cases in epileptic patients and a pathophysiological hypothesis. J Neurol Neurosurg Psychiatry 2001; 70: 459–463.
15. Hashimoto Y, Takanashi J, Kaiho K, et al. A splenial lesion with transiently reduced diffusion in clinically mild encephalitis is not always reversible. A case report. Brain Dev 2009; 31: 710–2.

Received: 03/03/2016
Accepted: 10/05/2016

CASE REPORT

A rare case of Ganglioneuroblastoma Encapsulated in Pheochromocytoma

Nathália Vieira Sousa[1,], Luísa Coelho Marques de Oliveira[1], Paulo José Oliveira Cortez[1], Vitor Engrácia Valenti[2], David Mathew Garner[3], Roseane de Souza Candido Irulegui[1], Dalmo Antônio Ribeiro Moreira[1,4]*

[1] Faculdade de Medicina de Itajubá, Av. Renó Júnior, 368 – São Vicente, Itajubá, MG, Brazil
[2] Programa de Pós-Graduação em Fisioterapia, Faculdade de Ciências e Tecnologia, UNESP, Rua Roberto Simonsen, 305, Presidente Prudente, SP, Brazil
[3] Department of Biological and Medical Sciences, Faculty of Health and Life Sciences, Oxford Brookes University, Gipsy Lane, Oxford OX3 0BP, United Kingdom
[4] Instituto Dante Pazzanese de Cardiologia, Av. Dr. Dante Pazzanese, 500, São Paulo, SP, Brazil
* Corresponding author: Faculdade de Medicina de Itajubá, Av. Renó Júnior, 368 – São Vicente, Itajubá, MG, Brazil; e-mail: nathaliavieira100@hotmail.com

Summary: Pheochromocytoma and Ganglioneuroblastoma are separate diseases and a rare combination in which the diagnosis can only be confirmed by pathological examination after tumor excision. We reported here a case of ganglioneuroblastoma encapsulated in pheochromocytoma. The patient is a woman, 73 years old, hypertensive, with hypothyroidism, associated for 15 years with hypercholesterolemia and hypertriglyceridemia, which had frequent complaints of low back pain. She underwent magnetic resonance and the findings were consistent with the diagnosis of pheochromocytoma. After surgery, anatomic, pathologic and immunohistochemistry analysis confirmed the diagnosis of pheochromocytoma composed by small ganglioneuroblastoma representation with the identification of small focus of infiltration of the adrenal capsule and adipose tissue by pheochromocytoma. This rare association can instigate the discussion of methods of diagnosis, more effective and more appropriate treatments for each patient.

Keywords: *Pheochromocytoma; Ganglioneuroblastoma; Abdominal Neoplasms*

Introduction

Prior to 2000, only six cases of a compound tumor containing Pheochromocytoma and Ganglioneuroblastoma were reported (1–3). In this context, we herein present a rare case of a patient with ganglioneuroblastoma encapsulated in pheochromocytoma.

Case Report

Woman, white, 76 years old, 68.2 kg, married, born in Codisburgo (MG, Brazil) and living in Contagem (MG), diagnosed with hypertension when she was 66 years old. History of hypothyroidism for 15 years associated with hypercholesterolemia and hypertriglyceridemia. After treatment with common analgesics for several years, the patient persisted with complaints of constant high intensity back pain. Due to noncompliance to conventional medical treatment it was suggested to undertake magnetic resonance image (MRI) of the lumbosacral spine to perform better orthopedic workup. An ovoid structure was detected in the left adrenal gland. Consequently, an additional MRI confirmed the presence of a rounded mass lesion, heterogeneous, clear limits, located on the left adrenal gland, measuring 2.0 × 2.0 cm. There was important and heterogeneous contrast uptake in the tumor, these results very compatible with a diagnosis of pheochromocytoma. The patient complained of sporadic headaches and dyspnea on exertion, however, she denied dizziness, blurred vision, cold sweats or palpitations. She had been submitted to cardiovascular workup, scintigraphy and coronary angiography for further clarification of atypical chest pain. Nevertheless, coronary atheromatosis was not diagnosed.

Tab. 1: Urinary fractions epinephrine, norepinephrine, dopamine, normetanephrine, metanephrine. free cortisol and vanillylmandelic acid.

Variable	Value	Reference
Epinephrine	33.41 mcg/24h	<20
Norepinephrine	54.72 mcg/24h	<75
Dopamine	216.29 mcg/24h	<400
Normetanephrine	381.60 mcg/24h	90–440
Metanephrine	82.22 mcg/24h	50–340
Cortisol	41.80 mcg/24h	10–90
Vanillylmandelic acid	2.20 mg/24h	<6.8

http://dx.doi.org/10.14712/18059694.2016.92

On physical examination the patient was in good general condition, anxious and was typically colored. For the evaluation of the heart, the heart rhythm was regular with normal sounds, heart rate of 64 bpm, blood pressure 130/80 mmHg in the supine position and 120/85 mmHg in standing position. The arterial pulses were rhythmic, symmetrical with excellent amplitude; absence of signals compatible with venous insufficiency.

In laboratory tests, the electrocardiogram recorded-regular sinus rhythm with P waves, QRS complexes and normal repolarization. In the echocardiography examination, the size of the left atrium, the ventricular function assessed by ejection fraction and ventricular myocardial thickness

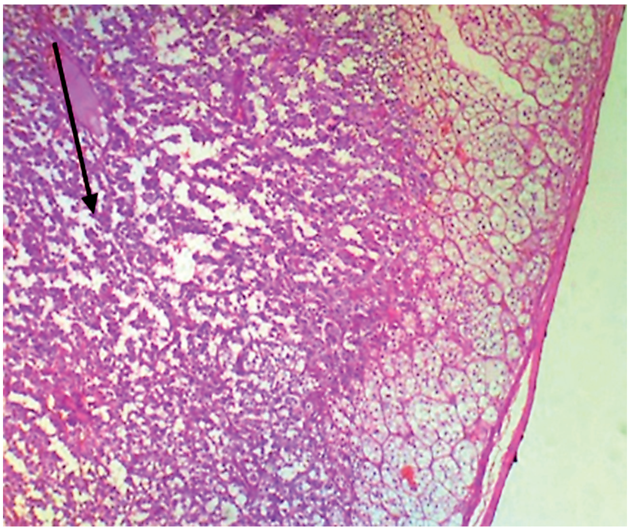

Fig. 1: Pre-surgery 131 meta-iodo-benzylguanidine scintigraphy. Optical microscopy showing neoplastic infiltration in the cortex of the adrenal gland.

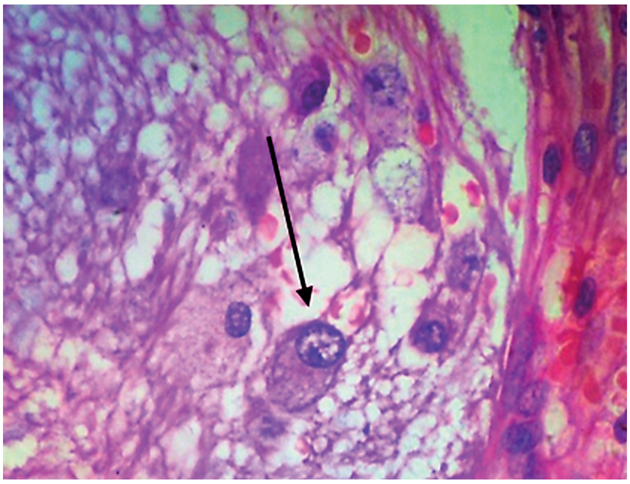

Fig. 2: Optical microscopy showing neural differentiation compatible with neoplasm of the nerve fibers and neurons.

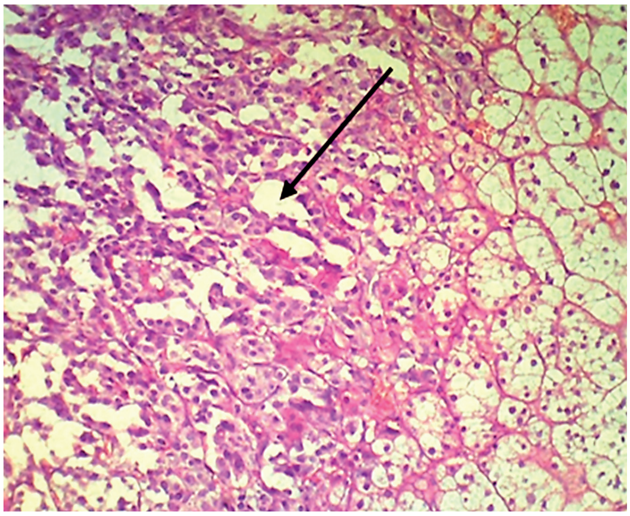

Fig. 3: Optical microscopy, at higher magnifications, showing neural differentiation consistent with neoplasia neurons and nerve fibers.

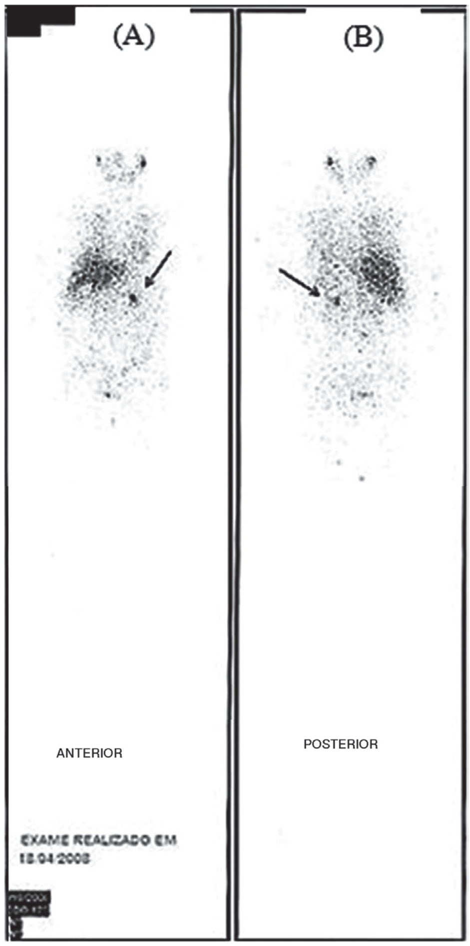

Fig. 4: Pre-surgical meta-iodo-benzylguanidine scintigraphy after tumor resection.

(septum and free wall) and ventricular systolic and diastolic volumes were normal.

Catecholamine levels and urinary fractions were performed as epinephrine, norepinephrine, dopamine and urinary fractions, as normetanephrine, metanephrine; free cortisol and vanillylmandelic acid (Table 1).

After implementation the magnetic resonance imaging of the abdomen, abdominal scintigraphy was performed with 131 meta-iodo-benzylguanidine (MIBG) scintigraphy, which revealed the lesions illustrated in Figure 1, consistent with the presence in the left adrenal gland of pheochromocytoma projection. The diagnosis was confirmed and surgery scheduled.

A tumor infiltration adjacent to the recumbent fat tissue induced subcapsular hemorrhage, in an attempt to resect this tissue it bled and a surgical procedure was necessary.

The preoperative preparation of patients began with prazosin, prescribed in the prior week in order to conduct adrenergic blockade. There was suspension of an antihypertensive drug (atenolol) that was already administered to the patient, but due to recurrence of migraine it had been replaced by the beta blocker metoprolol 25 mg/day. During surgery xyphopubic incision was performed for extended access to the abdominal cavity and planned subtotal adrenalectomy. The adrenalectomy was decided by the surgical team in order to assess more clearly the tumor extension. During surgery the patient presented a hypertensive peak corrected with use of sodium nitroprusside. Furthermore, there was splenic hemorrhage due to infiltration of surrounding tissue by the tumor, and it was necessary to continue to complete a splenectomy. After surgery, she progressed with hypovolemia and anemia, inducing hypovolemic shock, with the need for fluid infusion and transfusion of red blood cells. The histopathological analyzes and immunohistochemistry (Figure 2 and 3) confirmed the diagnosis of pheochromocytoma composed by a small intermediate ganglioneuroblastoma representation with the identification of small focus of infiltration of the adrenal capsule and adipose tissue by pheochromocytoma.

One year following surgery, another MIBG scintigraphy was undertaken, which resulted in no abnormal fixation of the radiopharmaceutical in the whole body extension, excluding tumor recurrence (Figure 4). Currently, five years after surgical treatment she is asymptomatic and without the need for antihypertensive medication.

Considerations

In this case study a difficulty was reported and it was necessary to administer use of sodium nitroprusside, the drug precursor of nitric oxide that causes vasodilation and systemic venous blood (4). This infusion rapidly reduced blood pressure, reversing the blood pressure elevations, which increase the morbidity and mortality of surgical procedure. Alternatively, the sharp fall in risk of plasma catecholamine levels after tumor resection exposed the patient to a hemodynamic instability, which progressed to hypovolemic shock and death. That is why constant monitoring of blood pressure during surgery is critical in this class of patients.

Composite pheochromocytoma–ganglioneuroblastoma is an extremely rare tumor (1, 6–12), given this unusual association that sparked interest in reporting the case; we confirm its importance to be source of studies and possible new treatments.

References

1. Okumi M1, Ueda T, Ichimaru N, Fujimoto N, Itoh K. A case of composite pheochromocytoma-ganglioneuroblastoma in the adrenal gland with primary hyperparathyroidism. HinyokikaKiyo 2003; 49: 269–72.
2. Santos J, Paiva I, Carvalheiro M. Pheochromocytoma: updates in diagnosis and treatment. Rev Port Endocrinol Diabetes Metabol 2009; 1: 99–111.
3. Kimura N, Miura Y, Miura K. Adrenal and retroperitoneal mixed neuroendocrine-neural tumors. Endocr Pathol 1991; 2: 139–14.
4. Valenti VE, Ferreira C, Meneghini A, et al. Evaluation of baroreflex function in young spontaneously hypertensive rats. Arq Bras Cardiol 2009; 92: 205–15.
5. Bravo EL, Tagle R. Pheochromocytoma: state-of-the-art and future prospects. Rev Endocr 2003; 24: 539–53.
6. Shida Y, Igawa T, Abe K, et al. Composite pheochromocytoma of the adrenal gland: a case series. BMC Res Notes 2015; 8: 257.
7. Nigawara K, Suzuki T, Onodera T, et al. Watery diarrhea, hypokalemia, achlorhydria syndrome due to recurrent malignant pheochromocytoma. Nihon Naibunpi Gakkai Zasshi 1987; 63: 923–33.
8. Nigawara K, Suzuki T, Tazawa H, et al. A case of recurrent malignant pheochromocytoma complicated by watery diarrhea, hypokalemia, achlorhydria syndrome. J Clin Endocrinol Metab 1987; 65: 1053–6.
9. Thiel EL, Trost BA, Tower RL. A composite pheochromocytoma/ganglioneuroblastoma of the adrenal gland. Pediatr Blood Cancer 2010; 54: 1032–4.
10. Prejbisz A, Harazny J, Szymanek K, et al. 7D.07: Retinal arteriolas structure in patients with pheochromocytoma. J Hypertens 2015; 33 Suppl 1: e102.
11. Puar T, van Berkel A, Gotthardt M, et al. Genotype-Dependent Brown Adipose Tissue Activation in Patients With Pheochromocytoma and Paraganglioma. J Clin Endocrinol Meta 2016; 101(1): 224–32.
12. Loper H, Kant R, Olson J, Streeten E, Munir K. Invasive phaeochromocytoma presenting as a right atrial mass. Lancet Diabetes Endocrinol 2015; pii: S2213-8587(15)00466-0.

Received: 16/10/2015
Accepted: 02/03/2016

CASE REPORT

Abnormal Origin and Course of the Accessory Phrenic Nerve: Case Report

George Paraskevas[1,*], *Konstantinos Koutsouflianiotis*[1], *Panagiotis Kitsoulis*[2], *Ioannis Spyridakis*[1]

[1] Department of Anatomy, Faculty of Medicine, Aristotle University of Thessaloniki, Thessaloniki, Greece
[2] Department of Anatomy, Histology and Embryology, Faculty of Medicine, University of Ioannina, Ioannina, Greece
* Corresponding author: Department of Anatomy, Faculty of Medicine, Aristotle University of Thessaloniki, Thessaloniki, Greece, PO Box: 300, Postal Code: 54124; e-mail: g_paraskevas@yahoo.gr

Summary: In the current cadaveric study an unusual sizeable accessory phrenic nerve (APN) was encountered emerging from the trunk of the supraclavicular nerves and forming a triangular loop that was anastomosing with the phrenic nerve. That neural loop surrounded the superficial cervical artery which displayed a spiral course. The form of a triangular loop of APN involving the aforementioned artery and originating from the supraclavicular nerve to the best of our knowledge has not been documented previously in the literature. The variable morphological features of the APN along with its clinical applications are briefly discussed.

Keywords: *Phrenic nerve; Accessory; Variation; Applications*

Introduction

The accessory phrenic nerve (APN) as it is well known constitutes a slender branch arising from the fifth cervical ventral ramus via the nerve to the subclavius, lying lateral to the phrenic nerve (PN) and descending posterior or sometimes anterior to the subclavian vein. Ultimately the APN joins the PN usually near the first rib or beyond the base of the neck inside the thoracic cavity (1, 2). The APN's incidence displays a great variability ranging between 17.6% in German population as reported by Felix in 1922 (3) and 75% (4). Apart from APN's main origin from the nerve to subclavius it can take its origin from other sources such as ansa cervicalis, nerve to sternothyroid, supraclavicular nerve, roots of brachial plexus, spinal accessory or even hypoglossal nerve (5, 6). APN constitutes a relatively neglected neural structure, since much greater attention has been paid to PN's anatomy. The APN is at risk after thoracic surgical procedures, subclavian vessel catheterization, and supraclavicular brachial plexus blocks.

In the current study, we present a very rare variant of the APN, that combines a rare origin from the supraclavicular nerve and an unusual loop around the superficial cervical artery.

Case report

During routine gross anatomy course dissection, we came across a very rare variant of a neural loop involving an arterial trunk in the cervical region of a 75-year-old formalin-fixed male cadaver, whose cause of death was not related to the current study. After careful removal of the skin, cervical fasciae, and sternocleidomastoid muscle, we encountered an unusual nerve arising from the trunk of the left supraclavicular nerves just after it emerged from the posterior border of the left sternocleidomastoid muscle at a distance of 0.9 cm from Erb's point. Erb originally described this point as "a circumscribed point about 2–3 cm above the clavicle somewhat outside of the posterior border of the sternomastoid muscle" (7). However, we utilized as a landmark the "punctum nervosum" that is situated ap-

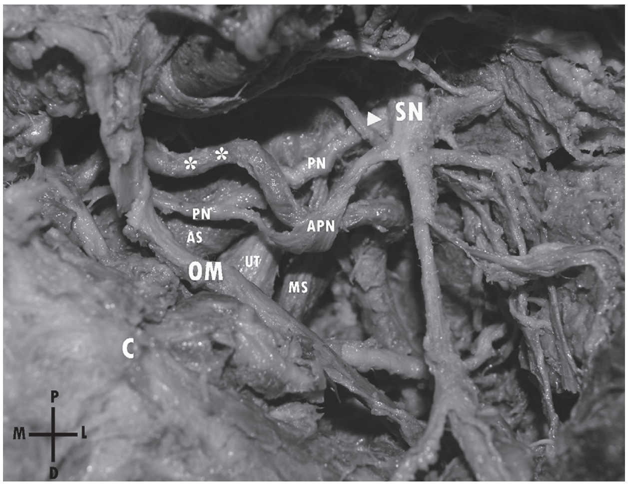

Fig. 1: Photograph of the left posterior triangle of the neck, where an atypical loop is observed interconnecting the accessory phrenic nerve (APN) with the ipsilateral phrenic nerve (PN). The APN/PN loop is seen surrounding the left superficial cervical artery (asterisks). (SN: supraclavicular nerve, OM: omohyoid muscle, C: clavicle, AS: Anterior scalene muscle, MS: Middle scalene muscle, UT: upper trunk of brachial plexus, P: proximal, D: distal, M: medial, L: lateral).

ACTA MEDICA (Hradec Králové) 2016; 59(2):70–71
http://dx.doi.org/10.14712/18059694.2016.55

proximately at the midpoint of the posterior border of the sternocleidomastoid muscle (8). A sizable APN was identified here, which after a short course of 1.6 cm divided into a proximal ascending and a distal descending branch both of which communicated with the left PN proximal to the intermediate tendon of the ipsilateral omohyoid muscle. This triangular neural loop surrounded the left superficial cervical artery (Fig. 1). No other associated anatomical variations or scars from previous surgical procedures were present. The origin, course, and morphology of this neural APN/PN loop and its relationship to the surrounding anatomical structures were photographed during the dissection.

Discussion

The APN is an inconstant nerve with a highly variable incidence. Its frequency in cadaveric studies was 61.8–65% (from Aycock et al as cited by Kelley) (5, 9). In other studies the incidence ranged from 2.63% (10) to 80.9% (5, 6, 10, 11). Given these figures APN could be regarded as a constant neural element and not a variant (5). A crucial point is the precise APN's definition. Loukas et al decided that all nerves contributing to the PN after it had crossed the anterior scalene muscle would be considered as APN (5). According to Hollinshead's textbook of Anatomy when two parts of the PN exist coursing parallel to each other for a variable distance on the anterior scalene muscle, usually the lower is called APN (12). Banneheka identified the additional contributions to PN passing anterior to the subclavian vein (in 28.7%) as APN, whereas those found passing posterior to the subclavian vein were termed secondary PNs (in 19.8%) (13). As regards its origin, APN usually arises from the nerve to subclavius (45.8–60.6%) and the ansa cervicalis (12.1–16.6%) (5, 6, 14). The APN may also originate from the upper trunk of the brachial plexus, the nerve to sternohyoid, C4 root or the supraclavicular nerve (4–16.6%) (5, 6). Uncommon origins include the hypoglossal, spinal accessory and vagus nerves (5, 14).

APN usually joins the PN within the thorax (67.7%) and not at the root of the neck (32.3%) as is usually reported (5). The loop between the APN and PN may include a vessel, such as the internal thoracic artery, which may complicate harvesting of that artery during coronary artery bypass grafting. Such a loop was detected in 38.4% by Loukas et al (5), whilst Nayak et al found none (6). An APN/PN loop including the subclavian vein was observed in 34.4–45.5% of cases (5, 6). This loop can be damaged during subclavian vein catheterization. An APN/PN loop was observed involving the subclavian artery in 1.11% of cases (6).

An APN/PN loop including the superficial cervical artery as noted in the current study has not documented in the literature to the best of our knowledge. The formation of a nerval loop including an artery is an uncommonly detected condition. It has been postulated that with the establishment of the muscular system during embryological development, the nerve pattern becomes fixed and does not adjust itself to the more variable arteries when they tend to revert to their earlier primate positions. This constitutes an explanation for the condition where a nerve is perforated by an artery (15).

Although PN's lesion during subclavian vein catheterization is well known and established in the literature (16), APN could be damaged during subclavian vein's cannulation especially in cases where it is situated anterior to that vein. Moreover, the APN is vulnerable during supraclavicular exposures performed for thoracic outlet syndrome. It has been reported that permanent or transient diaphragmatic dysfunction after scalenectomy could be due not only to PN's injury but to APN's injury as well (17).The APN's presence can explain the preservation of forced vital capacity even in patients after a supraclavicular block of the brachial plexus (18). The presence of an APN may also explain why bilateral PNs transection may be compatible with life (19).

Conclusion

The APN may be less of a variant and more of a constant neural structure. A rare origin from the supraclavicular nerve trunk encircling the superficial cervical artery is described.

References

1. Berry M, Bannister LH, Standring SM, et al. Nervous System. In: Williams PL, eds. Gray's Anatomy. Edinburgh: Churchill Livingstone, 1995: 1265–6.
2. Basmajian JV. Grant's Method of Anatomy. 8th ed. Baltimore: Williams and Wilkins Co, 1971: 560.
3. Kikuchi T. A contribution to the morphology of the ansa cervicallis and the phrenic nerve. Kaibogaku Zasshi 1979; 45: 242–81.
4. Bergman RA, Afifi AK, Miyauchi R, et al. Illustrated Encyclopedia of Human Anatomic Variation: Opus III: Nervous System: Plexuses, Phrenic Nerve. http://www.anatomyatlases.org. Accessed on 30 August 2015.
5. Loukas M, Kinsella CR, Louis RG, Gandhi S, Curry B. Surgical anatomy of the accessory phrenic nerve. Ann Thorac Surg 2006; 82: 1870–5.
6. Nayak SR, Krishnamurthy A, Prabhu LV, et al. Incidence of accessory phrenic nerve and its clinical significance: a cadaveric study. Acta Med 2008; 51(3): 181–4.
7. Erb W. Handbook of Electro-Therapeutics (translation: L Putzel). New York: William Wood and Co, 1883: 122–4.
8. Frank DK, Wenk E, Stern JC, Gottlieb RD, Moscatello AL. A cadaveric study of the motor nerves to the levator scapulae muscle. Otolaryngol Head Neck Surg 1997; 117: 671–80.
9. Kelley WO. Phrenic nerve paralysis; special consideration of the accessory phrenic nerve. J Thorac Surg 1950; 19: 923–8.
10. Dayal S, Ky M. The variations in the roots of origin of the phrenic nerve. J MGIMS 2009; 14(2): 24–7.
11. Fazan VPS, Amadeu ADS, Caleffi AL, Filho OAR. Brachial plexus variations in its formation and main branches. Acta Cir Bras 2003; 18(suppl. 5): 14–8.
12. Rosse C, Gaddum-Rose P. Hollinshead's Textbook of Anatomy. 5th ed. Philadelphia: Lippincott-Raven, 1997: 720–1.
13. Banneheka S. Morphological study of the ansa cervicalis and the phrenic nerve. Anat Sci Int 2008; 83: 31–44.
14. Yano K. Zur Anatomie und Histologie des Nervus phrenicus und soggenanten Nebenphrenicus, nebst Bemerkungen uber ihre Verbindung mit Sympathicus. Folia Anat Jpn 1925; 6: 247–90.
15. Miller RA. Observations upon the arrangement of the axillary artery and brachial plexus. Am J Anat 1939; 64: 143–63.
16. Paraskevas GK, Raikos A, Chouliaras K, Papaziogas B. Variable anatomical relationship of phrenic nerve and subclavian vein:clinical implication for subclavian vein catheterization. Br J Anaesth 2011; 106(3): 348–51.
17. Sharma MS, Loukas M, Spinner RJ. Accessory phrenic nerve: a rarely discussed common variation with clinical implications. Clin Anat 2011; 24: 671–3.
18. Bigeleisen PE. Anatomical variations of the phrenic nerve and its clinical implication for supraclavicular block. Br J Anaesth 2003; 91(6): 916–7.
19. Vilensky JA. "C3, C4, C5, keep you alive" or do they? Clin Anat 2006; 19: 130–1.

Received: 02/09/2015
Accepted: 16/03/2016